Haverford College

Haverford Scholarship

2008

The Nature of CO Emission from z~6 Quasars

Desika Narayanan
Haverford College, dnarayan@haverford.edu

THE NATURE OF CO EMISSION FROM $z \sim 6$ QUASARS

Desika Narayanan,[1] Yuexing Li,[2] Thomas J. Cox,[2] Lars Hernquist,[2] Philip Hopkins,[2]
Sukanya Chakrabarti,[2,3] Romeel Davé,[1] Tiziana Di Matteo,[4] Liang Gao,[5]
Craig Kulesa,[1] Brant Robertson,[6,7] and Christopher K. Walker[1]

ABSTRACT

We investigate the nature of molecular gas emission from $z \sim 6$ quasars via the commonly observed tracer of H_2, carbon monoxide (CO). We achieve this by combining non-LTE radiative transfer calculations with merger-driven models of $z \sim 6$ quasar formation that arise naturally in Λ cold dark matter structure formation simulations. Motivated by observational constraints, we consider four representative $z \sim 6$ quasars formed in the halo mass range $\sim 10^{12}$–$10^{13}\ M_\odot$ from different merging histories. Our main results are as follows. We find that, owing to massive starbursts and funneling of dense gas into the nuclear regions of merging galaxies, the CO is highly excited during both the hierarchical buildup of the host galaxy and the quasar phase, and the CO flux density peaks between $J = 5$ and 8. The CO morphology of $z \sim 6$ quasars often exhibits multiple CO emission peaks which arise from molecular gas concentrations which have not yet fully coalesced. Both of these results are found to be consistent with the sole CO detection at $z \sim 6$, in quasar J1148+5251. Quasars which form at $z \sim 6$ display a large range of sight line–dependent line widths. The sight line dependencies are such that the narrowest line widths are when the rotating molecular gas associated with the quasar is viewed face-on (when the L_B is largest) and broadest when the quasar is seen edge-on (and the L_B is lowest). Thus, we find that for all models selection effects exist such that quasars selected for optical luminosity are preferentially seen to be face-on which may result in CO detections of optically luminous quasars at $z \sim 6$ having line widths narrower than the median. The mean sight line–averaged line width is found to be reflective of the circular velocity of the host halo and thus scales with halo mass. For example, the mean line width for the $\sim 10^{12}\ M_\odot$ halo is $\sigma \sim 300$ km s^{-1}, while the median for the $\sim 10^{13}\ M_\odot$ quasar host is $\sigma \sim 650$ km s^{-1}. Depending on the host halo mass, approximately 2%–10% of sight lines in our modeled quasars are found to have narrow line widths compatible with observations of J1148+5251. When considering the aforementioned selection effects, these percentages increase to 10%–25% for quasars selected for optical luminosity. When accounting for both temporal evolution of CO line widths in galaxies, as well as the redshift evolution of halo circular velocities, these models can self-consistently account for the observed line widths of both submillimeter galaxies and quasars at $z \sim 2$. Finally, we find that the dynamical mass derived from the *mean* sight line–averaged line widths provide a good estimate of the total mass and allow for a massive molecular reservoir, supermassive black hole, and stellar bulge, consistent with the local M_{BH}-M_{bul} relation.

Subject headings: cosmology: theory — early universe — galaxies: active — galaxies: formation —
galaxies: high-redshift — galaxies: individual (SDSS J1148+5251) — galaxies: ISM

1. INTRODUCTION

The discovery of extremely luminous quasars at $z \gtrsim 6$ via novel color-selection techniques demonstrates that massive galaxies and supermassive black holes formed very early in the universe (Fan et al. 2002, 2003, 2004). Observations of the dusty and molecular interstellar medium (ISM) in $z \sim 6$ galaxies can serve as a unique probe into the star formation process in the first collapsed objects and help quantify the relationship between star formation and black hole growth when the universe was less than a billion years old (e.g., Wang et al. 2007; for a recent review, see Solomon & Vanden Bout 2005). Serving as a proxy for observationally elusive molecular hydrogen (H_2), rotational transitions

in tracer molecules such as ^{12}CO (hereafter CO), HCN, and HCO$^+$ can provide diagnostics for the physical conditions in the star-forming giant molecular clouds (GMCs) of high-redshift galaxies (e.g., Bertoldi et al. 2003a, 2003b; Carilli et al. 2005; Riechers et al. 2006a; Walter et al. 2003).

The highest redshift quasar that has been found, SDSS J1148+5251 (hereafter J1148+5251) at $z = 6.42$ (Fan et al. 2003), is an extremely bright object with bolometric luminosity $\sim 10^{14}\ L_\odot$ and is thought to be powered by accretion onto a supermassive black hole of mass $\sim 10^9\ M_\odot$ (Willott et al. 2003). Bertoldi et al. (2003a) measured a far-infrared luminosity of $1.3 \times 10^{13}\ L_\odot$, which if powered solely by starburst-heated dust, corresponds to an exceptional star formation rate of $\sim 3000\ M_\odot$ yr^{-1}.

Pioneering CO observations of J1148+5251 have revealed a great deal concerning the molecular ISM in the host galaxy of this $z \sim 6$ quasar. Through multiline observations and large velocity gradient (LVG) radiative transfer modeling, Bertoldi et al. (2003b) found that the CO flux density peaks at the $J = 6$ level of CO, indicative of the warm and dense conditions characteristic of vigorous star formation. A measured molecular gas mass of $M_{H_2} \approx 10^{10}\ M_\odot$ shows that J1148+5251 plays host to a large reservoir of molecular gas (Bertoldi et al. 2003b; Walter et al. 2003). Subsequent high-resolution observations with the Very Large Array (VLA) by Walter et al. (2004) discovered that the

[1] Steward Observatory, University of Arizona, 933 North Cherry Avenue, Tucson, AZ, 85721.
[2] Harvard-Smithsonian Center for Astrophysics, 60 Garden Street, Cambridge, MA 02138.
[3] NSF Postdoctoral Fellow.
[4] Carnegie Mellon University, Department of Physics, 5000 Forbes Avenue, Pittsburgh, PA 15213.
[5] Institute for Computational Cosmology, Department of Physics, University of Durham, South Road, Durham, DH1 3LE, UK.
[6] Kavli Institute for Cosmological Physics and Department of Astronomy and Astrophysics, University of Chicago, 933 East 56th Street, Chicago, IL 60637.
[7] Spitzer Fellow.

CO emission in this galaxy is extended on scales of 2.5 kpc and is resolvable into two emission peaks separated by 1.7 kpc, with each peak tracing $\sim 5 \times 10^9 \ M_\odot$ of molecular gas. These observations suggest that J1148+5251 is a merger product (Walter et al. 2004; Solomon & Vanden Bout 2005).

CO observations of J1148+5251 have presented challenges for models of galaxy formation as well. For example, dynamical mass estimates from observed CO line widths are not able to account for the presence of a $\sim 10^{12} \ M_\odot$ stellar bulge as would be predicted by the present-day $M_{\rm BH}$-$M_{\rm bul}$ relation, suggesting that the central supermassive black hole could have grown in part before the host galaxy (Walter et al. 2004). In contrast, the presence of heavy elements (Barth et al. 2003) and significant CO emission (Bertoldi et al. 2003b; Walter et al. 2003, 2004) imply that the ISM has been significantly enriched with metals from early and abundant star formation. Recent theoretical arguments have additionally proposed that a relation between black hole mass and stellar bulge mass is a natural consequence of AGN feedback in galaxies (Di Matteo et al. 2005, 2007; Hopkins et al. 2007c; Sijacki et al. 2007) and that this relation shows only weak (~ 0.3–0.5 dex) evolution in galaxies from redshifts $z = 0$ to 6 (Robertson et al. 2006b, 2006c; Hopkins et al. 2007c).

Numerical simulations can offer complementary information to observations of $z \sim 6$ quasars by providing a framework for the formation and evolution of $z \sim 6$ quasars and the relationship between the star-forming ISM in these galaxies and observed CO emission. Calculations by Springel et al. (2005a, 2005b) have found that galaxy mergers serve as a viable precursor for quasar formation. Strong gaseous inflows driven by tidal torques on the gas (e.g., Barnes & Hernquist 1991, 1996) can fuel nuclear starbursts (e.g., Mihos & Hernquist 1994, 1996) and feed the growth of central, supermassive black holes (Di Matteo et al. 2005); subsequent feedback from the AGN can lift the veil of obscuring gas and dust and, along numerous sight lines, reveal an optically bright quasar (Hopkins et al. 2005a, 2005d).

More recently, Li et al. (2007) have proposed a merger driven model for quasar formation at $z \sim 6$ which fits naturally into a ΛCDM framework. By performing numerical simulations which simultaneously account for black hole growth, star formation, quasar activity, and host spheroid formation, these authors found that galaxy mergers in early $\sim 10^{13} \ M_\odot$ halos can result in the formation of bright quasars at $z \sim 6$. The quasars in these simulations exhibit many properties similar to the most luminous quasars at $z \sim 6$, including both observables, such as the rest-frame B-band luminosity, and inferred characteristics (e.g., the central black hole mass and bolometric luminosity). These simulations can thus serve as a laboratory for investigating the properties of the ISM in the first quasars, as well as the relation between CO emission and star formation at early epochs.

In order to quantitatively couple these models with CO observations, molecular line radiative transfer calculations are necessary. Recent works by Narayanan et al. (2006a, 2006b) have developed a methodology for simulating molecular line transfer on galaxy-wide scales. Here, we aim to investigate the plausibility of $z \sim 6$ quasar formation in massive $\sim 10^{12}$–$10^{13} \ M_\odot$ halos in a hierarchical structure formation scenario by modeling the observed CO emission from these high-redshift sources. We achieve these means by coupling the non-LTE radiative transfer codes of Narayanan et al. (2006a, 2006b) with the hierarchical $z \sim 6$ quasar formation models of Li et al. (2007). We make quantitative predictions for $z \sim 6$ quasars which form in halos with masses ranging from $\sim 10^{12}$ to $10^{13} \ M_\odot$ and provide interpretation for existing and future CO observations of $z \gtrsim 6$ quasars.

In § 2 we describe the numerical models employed. In § 3 we present the modeled CO excitation characteristics and luminosities. In § 4 we discuss the morphology of the CO gas. In § 5 we describe the derived emission line profiles and compare our models to observations of the only detected CO measurement in a $z \sim 6$ quasar, J1148+5251. In § 6 we use the model CO lines to investigate the usage of CO observations as dynamical mass indicators in the highest redshift quasars. We conclude with a discussion comparing the CO emission properties of our simulated quasar with other high-z galaxy populations in § 7 and summarize in § 8. Throughout this paper we assume a cosmology with $h = 0.7$, $\Omega_\Lambda = 0.7$, and $\Omega_m = 0.3$.

2. NUMERICAL METHODS

In order to capture the physics of early-universe quasar formation, simulations must have the dynamic range to faithfully track the evolution of the most massive halos within which these quasars reside (e.g., Haiman & Loeb 2001), as well as follow the stars, dark matter, ISM, and black holes in the progenitors of the quasar host galaxy. We have performed multiscale calculations, which include cosmological dark matter simulations in a volume of 3 Gpc^3 to identify the most massive halos, and subsequent hydrodynamic galaxy merger computations within these halos at higher resolution. The cosmological and galaxy merger simulations were implemented using the parallel, N-body/smoothed particle hydrodynamics (SPH) code GADGET-2 (Springel 2005). We then applied the non-LTE radiative transfer code, Turtlebeach (Narayanan et al. 2006a, 2006b), to the outputs of the hydrodynamic galaxy merger simulations to investigate the emission properties of the CO molecular gas in the resultant quasar. The quasar formation simulations and radiative transfer algorithms are described in detail in Li et al. (2007) and Narayanan et al. (2006a, 2006b), respectively, and we refer the reader to those works for more detail; here, we briefly summarize and focus on the aspects of the calculations directly relevant to this study.

2.1. Cosmological Simulations

Observational evidence suggests that quasars at $z \sim 6$ likely form in very massive ($\sim 10^{13} \ M_\odot$) halos. For example, quasars at $z \sim 6$ have an extremely low comoving space density of $n \approx 10^{-9} \ \mathrm{Mpc}^{-3}$ (e.g., Fan et al. 2003), comparable to the rarity of massive $\sim 10^{13} \ M_\odot$ halos at $z \sim 6$. Further evidence comes from black hole mass–halo mass correlations and theoretical arguments relating quasar luminosity and halo mass (Lidz et al. 2006). In addition, recent numerical simulations by Pelupessy et al. (2007) have suggested that the buildup of supermassive $\sim 10^9 \ M_\odot$ black holes by $z \sim 6$ may require galaxy mergers in extremely rare $\gtrsim 10^{13} \ M_\odot$ halos. The strongest evidence for high-redshift quasar formation in massive halos comes from recent SDSS clustering measurements by Shen et al. (2007) which indicate that the minimum mass for high-redshift quasar hosts is ~ 6–$9 \times 10^{12} \ M_\odot$. While these arguments are suggestive, they are not conclusive. Thus, one major goal of this work is to further investigate the hypothesis that $z \sim 6$ quasars live in high-mass halos and constrain the range of host halo masses for these sources by comparing their simulated CO emission to observations. To this end, we have simulated four quasars which form hierarchically through numerous mergers in massive halos ranging in mass from $\sim 10^{12}$ to $10^{13} \ M_\odot$.

In order to simulate the large subvolume of the universe necessary to track the evolution of massive halos and formation of $z \sim 6$ quasars, as well as achieve a reasonable mass resolution at the same time, we performed the structure formation simulation

TABLE 1
Quasar Models

Name[a]	z[b]	$M_{\rm vir}$[c] ($10^{12}\ M_\odot$)	$V_{\rm vir}$[d] (km s^{-1})	$M_{\rm BH}$[e] ($10^9\ M_\odot$)	$L_{\rm bol}({\rm peak})$[f] ($10^{13}\ L_\odot$)	$\tau_{\rm QSO}(L_{\rm bol} \geq 10^{13}\ L_\odot)$[g] (Myr)
Q1..................	6.5	7.7	626.4	2.0	2.0	55.5
Q2..................	5.6	3.8	467.9	1.0	5.0	22.3
Q3..................	7.2	1.5	340.7	0.2	1.5	4.0
Q4..................	5.5	8.1	593.2	0.4	1.1	21.9

[a] Name of quasar model.
[b] Redshift of the quasar at peak accretion activity.
[c] Virial mass of the quasar host halo, assuming overdensity $\Delta = 200$.
[d] Virial velocity of the quasar host halo, assuming overdensity $\Delta = 200$.
[e] Black hole mass of the quasar.
[f] Peak bolometric luminosity of the quasar.
[g] Quasar lifetime for $L_{\rm bol} \geq 10^{13}\ L_\odot$.

with a multigrid procedure similar to Gao et al. (2005). We first ran a uniform resolution simulation of a 3 Gpc^3 volume, with an effective mass and spatial resolution of $m_{\rm dm} \sim 1.3 \times 10^{12}\ M_\odot$ and $\epsilon \sim 125\ h^{-1}$ kpc (comoving softening length), respectively, with initial conditions generated by CMBFAST (Seljak & Zaldarriaga 1996). We assumed a σ_8 of 0.9 (although see Li et al. [2007] for a discussion of the implications of other choices for the cosmological parameters).

We then used a friends-of-friends group finder in order to seek out candidate massive halos within which early quasars form. Anticipating that these rare quasars will be progenitors of massive objects today, we identified the most massive halos at $z = 0$ and then resimulated the evolution of these objects and their immediate environment at a much higher mass and force resolution assuming an initial redshift of $z = 69$. The final effective resolutions of the halo evolution simulations were $m_{\rm dm} \sim 2.8 \times 10^8\ M_\odot$ and $\epsilon \sim 5\ h^{-1}$ kpc.

The merger tree of the halos was extracted from the simulations in order to provide information concerning the masses of the largest contributing progenitors to the halo mass and allow us to reconstruct the hierarchical buildup of the quasar host galaxy. We considered groups that contribute at least 10% of the halo mass as progenitors in the merger history resulting in, e.g., seven progenitors for the most massive halo simulated. Table 1 lists the properties of all the resultant quasars.

The discussion throughout this paper will largely focus on quasars Q1–Q3, which formed hierarchically in the cosmological simulations. Quasar Q4 is a binary coplanar merger specially simulated for studying the dependence of the CO emission properties on merger history and will be discussed only in § 5.2.

2.2. Galaxy Merger Simulations

To derive the physical properties of the $z \sim 6$ quasar host galaxies, we resimulated their merger trees hydrodynamically using GADGET-2. GADGET-2 utilizes a fully conservative SPH formulation which allows for an accurate handling of discontinuities (Springel & Hernquist 2002). The code accounts for radiative cooling of the gas (Katz et al. 1996; Davé et al. 1999) and a multiphase description of the ISM that includes cold clouds in pressure equilibrium with a hot, diffuse gas (e.g., McKee & Ostriker 1977; see also Springel & Hernquist 2003a). Star formation is constrained by observations of local galaxies and follows the Kennicutt-Schmidt laws (Kennicutt 1998; Schmidt 1959; Springel & Hernquist 2003b). The progenitor galaxies had dark matter halos initialized to follow a Hernquist (1990) profile, and the virial properties are scaled to be appropriate for cosmological redshifts (Robertson et al. 2006c).

Black holes in the simulations are realized through sink particles that accrete gas following a Bondi-Hoyle-Lyttleton parameterization (Bondi & Hoyle 1944; Bondi 1952; Hoyle & Lyttleton 1939). To model feedback from central black holes, we assume that 0.5% of the accreted mass energy is reinjected into the ISM as thermal energy (Di Matteo et al. 2005; Springel et al. 2005a, 2005b). This formulation for AGN feedback in galactic-scale simulations has been shown to successfully reproduce X-ray emission patterns in galaxy mergers (Cox et al. 2006a), observed quasar luminosity functions and lifetimes (Hopkins et al. 2005a, 2005b, 2005c, 2005d, 2006a, 2006b, 2007b, 2007e), the Seyfert galaxy luminosity function (Hopkins & Hernquist 2006), the $M_{\rm BH}$-σ_v relation (Di Matteo et al. 2005; Hopkins et al. 2007c; Robertson et al. 2006c), the bimodal galaxy color distribution (Springel et al. 2005b; Hopkins et al. 2006c, 2006d, 2007a), characteristic CO emission patterns in ultraluminous infrared galaxies (ULIRGs; Narayanan et al. 2006b), infrared colors of ULIRGs and $z \sim 2$ submillimeter galaxies with embedded AGNs (Chakrabarti et al. 2006, 2007), the kinematic structure of merger remnants (Cox et al. 2006b), and the SFR-HCN relation in galaxies (Narayanan et al. 2007a).

We assume that the black holes in these simulations formed from the first stars (e.g., Abel et al. 2002; Bromm & Larson 2004; Yoshida et al. 2006) and that the seed masses for the black holes are $200\ M_\odot$ at $z = 30$. Before the first progenitor galaxies entered the merger tree, their black holes grew at the Eddington limit, resulting in seed black hole masses of $\sim 10^4\ M_\odot$ at the time of the first merger. The black holes in the simulations are assumed to merge when their separation is less than a gravitational softening length ($30\ h^{-1}$ pc).

We model evolution of the CO emission in the quasars from $z \approx 8$ to 5, noting that the peak of the quasar activity is roughly $7 \gtrsim z \gtrsim 5.5$. The black hole luminosity outshines the stellar luminosity for a large range of redshifts, and it is this time that we refer to as the "quasar phase" for any given galaxy.

2.3. Evolution of Model Quasars

To aid in the discussion in the remainder of this work, we qualitatively describe the evolution of the most massive ($\sim 10^{13}\ M_\odot$) quasar host, although the results are general for all models considered in Table 1. The quasar host galaxy builds hierarchically, through seven major mergers between $z = 14.4$ and 8.5. Strong gravitational torques on the gas drive massive gaseous inflows, causing heavy accretion onto the central black hole(s) and triggering intense starbursts that typically form stars at a rate between $\sim 10^3$ and $10^4\ M_\odot {\rm yr}^{-1}$. The black holes accrete heavily as gas is funneled in toward the nuclear regions. Feedback from

the most massive central black hole then drives a powerful wind, creating numerous lines of sight along which the central quasar is no longer obscured, and the black hole luminosity outshines the stellar luminosity. The central supermassive black hole can be visible as an optically bright quasar ($L_{bol} > 10^{13} \ L_\odot$) for ~50 Myr (although less for lower mass quasar host galaxies; Table 1). The powerful quasar wind quenches the starburst and self-regulates the black hole growth. In the postquasar phase, the luminosity of the galaxy subsides, and it eventually evolves into a cD-like galaxy. More details concerning the evolution of the models presented here are discussed in Li et al. (2007).

2.4. *Molecular Line Radiative Transfer*

The CO emission properties were calculated using Turtlebeach, a three-dimensional non-LTE radiative transfer code, based on an expanded version of the Bernes (1979) algorithm (Narayanan et al. 2006a, 2006b). Our improvements focus on including a mass spectrum of GMCs in a subgrid manner, which allows us to more accurately model the molecular line radiation from the dense cores of molecular clouds, as well as the diffuse outer layers.

We build the emergent spectrum by integrating the equation of radiative transfer along various lines of sight,

$$I_\nu = \sum_{r_0}^{r} S_\nu(r) \left[1 - e^{-\tau_\nu(r)} \right] e^{-\tau_\nu(\text{tot})}, \qquad (1)$$

where I_ν is the frequency-dependent intensity, S_ν is the source function, r is the physical depth along the line of sight, and τ is the optical depth. The source function is dependent on the CO level populations which are assumed to be in statistical equilibrium, but not in LTE. This aspect of the calculation is important as the assumption of LTE often breaks down when considering the propagation of submillimeter-wave radiation through the molecular ISM.

We consider collisions with H_2, radiative excitation, and stimulated and spontaneous emission in determining the CO level populations. The radiative transfer is handled in a Monte Carlo manner, in which photon "packets" are emitted isotropically over 4π steradians. The frequencies are randomly drawn from the local line profile function which includes effects from the kinetic temperature and a microturbulent velocity field which we assume to have a constant value of 0.8 km s^{-1}. The strongly density-dependent collisional excitation rates are modeled by deriving the density distribution in a given cell from a mass spectrum of GMCs. In this formulation, we model the density distributions in the clouds as singular isothermal spheres with power-law index $p = 2$ (e.g., Walker et al. 1990), where the radius of each cloud is determined by the Galactic GMC mass-radius relation (e.g., Solomon et al. 1987; Rosolowsky 2005, 2006). Our results for higher lying CO transitions are particularly improved using this subgrid non-LTE approach. The molecular mass fraction of cold gas is assumed to be half, as motivated by local volume surveys (e.g., Keres et al. 2003). This resulted in molecular gas masses of 1–3 × 10^{10} $M_\odot$ in the model quasars.

Our methodology is an iterative one. A solution for the CO level populations is first guessed and provides the initial radiation field. We then calculate the mean intensity field in a Monte Carlo manner. The contributions of the radiation field and collisional excitation rates determine the updated level populations via rate equations, and the process is repeated until convergence.

We have benchmarked our radiative transfer codes against the published non-LTE line transfer tests of van Zadelhoff et al. (2002) and present the results in Narayanan et al. (2006a). Our approach in combining non-LTE radiative transfer calculations

with galaxy-scale hydrodynamic simulations has predicted CO morphologies, spatial extents, excitation levels, line widths, and intensities that are in good agreement with observations of local starbursts and galaxy mergers (Narayanan et al. 2006b; Narayanan et al. 2007b).

For the models presented here, 1×10^7 model photons were emitted per iteration. The mass spectrum of GMCs in each sub-grid cell considered clouds with a lower cutoff at $1 \times 10^4 \ M_\odot$ and an upper cutoff at $1 \times 10^6 \ M_\odot$, consistent with observed mass ranges of GMCs (e.g., Blitz et al. 2007). We calculated CO transitions across 10 levels at a time and assumed a uniform Galactic CO abundance of CO = $1.5 \times 10^{-4} \times H_2$ (Lee et al. 1996). We utilized collisional rate coefficients from the Leiden Atomic and Molecular Database (Schöier et al. 2005).

Throughout this work, we make predictions for CO transitions ranging from $J = 1$–0 through $J = 10$–9. One potential caveat regarding the lower lying (e.g., $J = 1$–0) transitions is that the low-density molecular gas in $z \sim 6$ quasars may be in a diffuse intracloud medium as is thought to be the case for local ULIRGs, rather than bound in GMCs (Downes & Solomon 1998). In our subgrid modeling of GMCs, we assume implicitly that the diffuse molecular gas is bound in the outer envelopes of GMCs which are characterized as singular isothermal spheres. The assumption of higher density gas residing in bound cloud cores is likely to be more robust. Recent studies show similarities between LIR/HCN ratios in both local GMCs and a large sample of ULIRGs. These similarities suggest that the high-density gas even in the nuclei of galaxy mergers is locked in cloud cores (Wu et al. 2005), similar to the simulations presented here. In this sense, our modeled environment of higher density gas is more reasonable, and predictions concerning higher lying transitions of CO (e.g., $J \gtrsim 3$) are more robust.

3. EXCITATION AND LUMINOSITY OF CO

The CO spectral energy distribution (SED) is the CO flux density emitted per rotational J state and thus provides a direct measure of the excitation characteristics of molecular gas (e.g., Weiß et al. 2005a). The shape and peak of the CO SED describe the relative number of molecules in a given rotational J state and serve as observable diagnostics of the underlying temperature and density of the emitting molecular gas. Here, we describe in detail the excitation characteristics of the most massive quasar host (Q1, $M \sim 10^{13} \ M_\odot$) and explicitly note when the lower mass models exhibit different properties. In Figure 1 we show the redshift evolution of the peak in the CO SED. Moreover, in Figure 2 we show representative CO SEDs for quasar Q1 at three redshifts during the quasar phase. The CO SEDs are averaged over three orthogonal viewing angles, although the SEDs derived from each individual angle are nearly identical.

Strong gravitational torques exerted on the gas by the multiple mergers drive massive amounts of cold gas into the central kilo-parsec, giving rise to densities as high as ~10^7 cm^{-3} in GMC cores at the beginning of the quasar phase ($z \sim 7$). The combination of these dense conditions and heating associated with the continued starburst cause the CO molecular gas to become highly excited. During this time, the peak of the CO SED rises to $J = 8$. Molecular gas in the central ~kiloparsec dominates the high-lying excitation. To place this in the context of active star-forming regions in the local universe, Weiß et al. (2005b) found the CO SED to peak at $J = 6$ in the nuclear region of starburst galaxy M82.

As energy input from the quasar begins to quench the starburst and dispel gas from the central regions, the star formation rate drops to ~10^2 $M_\odot$ yr^{-1}. Consequently, the peak excitation in
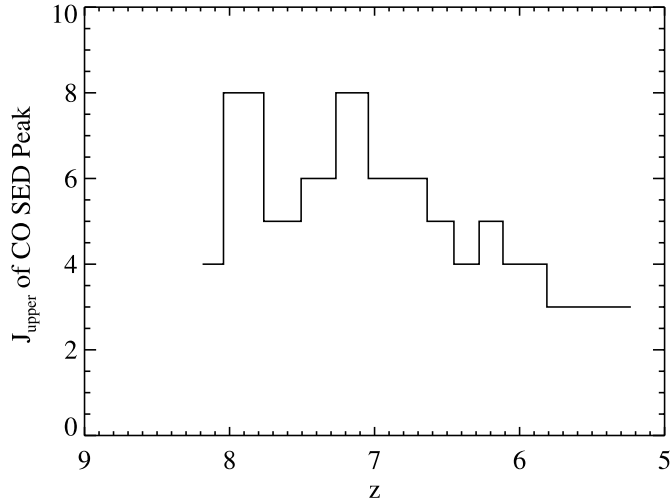
FIG. 1.—Upper rotational state (J_{upper}) of CO SED peak as a function of redshift for most massive quasar host, model Q1 (see Table 1). During the early, massive starburst, most of the CO is highly excited. During the height of the quasar phase, the peak in the CO excitation in our simulated galaxy ranges from $J = 8$ in the beginning of the quasar phase to $J = 5$ near the end. This is broadly consistent with observations of excited molecular gas in the sole CO detection at $z \sim 6$ (Bertoldi et al. 2003b). As the starburst subsides in the postquasar phase, lower temperatures and densities drive the peak in the CO SED down to $J \sim 3$.

the molecular gas rapidly drops to values more similar to local starbursts. During most of the quasar phase, the CO flux density in the simulated galaxy peaks at $J = 6$. This is consistent with the multiline observations and CO SED derivations by Bertoldi et al. (2003b), who find the CO flux density in J1148+5251 to peak at $J = 6$. In a merger-driven model for high-z quasars, the interplay between massive starbursts and feedback from central black holes is important in determining the observed CO excitation characteristics in galaxies like J1148+5251.

The peak of the CO flux density remains roughly constant through the height of the quasar phase. As feedback from the central black holes further extinguishes the nuclear starburst, fewer molecules are highly excited, and consequently, the relative flux density from higher J levels begins to drop. In Figure 2, the slope of the CO SED at levels higher than the turnover point is

seen to become steeper as the quasar evolves. When the accretion onto the central supermassive black hole subsides in the postquasar phase ($z \lesssim 6$), the star formation rate (SFR) drops to $\lesssim 50\ M_\odot\ \mathrm{yr}^{-1}$. The bulk of the molecular gas in this late stage of the galaxy's evolution is only moderately excited, and the peak in the CO SED declines to $J \approx 3$–4.

The trends discussed above are similar in models Q2 and Q3 (Table 1), although the overall normalization is slightly different. The CO SED of both the intermediate-mass and low-mass models (Q2 and Q3) peaks at $J = 6$ at the beginning of the quasar phase and settles at $J = 4$ as the starburst subsides. The lower excitation values in the lowest mass model owe to overall lower densities and star formation rates. For example, during the quasar phase, the SFR from model Q3 is $\sim 30\ M_\odot\ \mathrm{yr}^{-1}$.

Another way to view the excitation characteristics of the molecular gas is through the velocity-integrated CO luminosity (in units of K-km s^{-1}, where the K is the Rayleigh-Jeans temperature). In Figure 3 we show the normalized velocity-integrated CO($J = 1$–0, $J = 3$–2, $J = 6$–5, and $J = 9$–8) intensity as a function of redshift. We additionally plot the SFR, stellar luminosity, and black hole luminosity. The CO luminosity across all transitions decreases as the merger activity progresses, and the starburst reaches its peak. This is especially true of the high-J states which are typically excited by collisions in the starburst-heated gas. All CO transitions peak in integrated intensity early on, when the starburst has not consumed most of the available star-forming gas, and collisions help to sustain molecular excitation. As the starburst fades owing to a diminishing fuel supply, the intensity from the high-lying CO transitions (e.g., 6–5, 9–8) falls off rapidly while the lower J transitions experience a more moderate decline. In part, this owes to the fact that the lowering of gas temperatures and densities does not heavily affect the molecular excitation at $J = 1$. De-excitation of warm, dense star-forming gas additionally contributes to populating the lower J states. While the CO luminosity is only about half of its maximum value during the quasar phase, the bolometric luminosity of the galaxy peaks here as the central quasar becomes visible (Fig. 3, bottom).

4. MOLECULAR GAS MORPHOLOGY

In this section we discuss the CO morphology of the model quasar host galaxies through their evolution. The discussion is
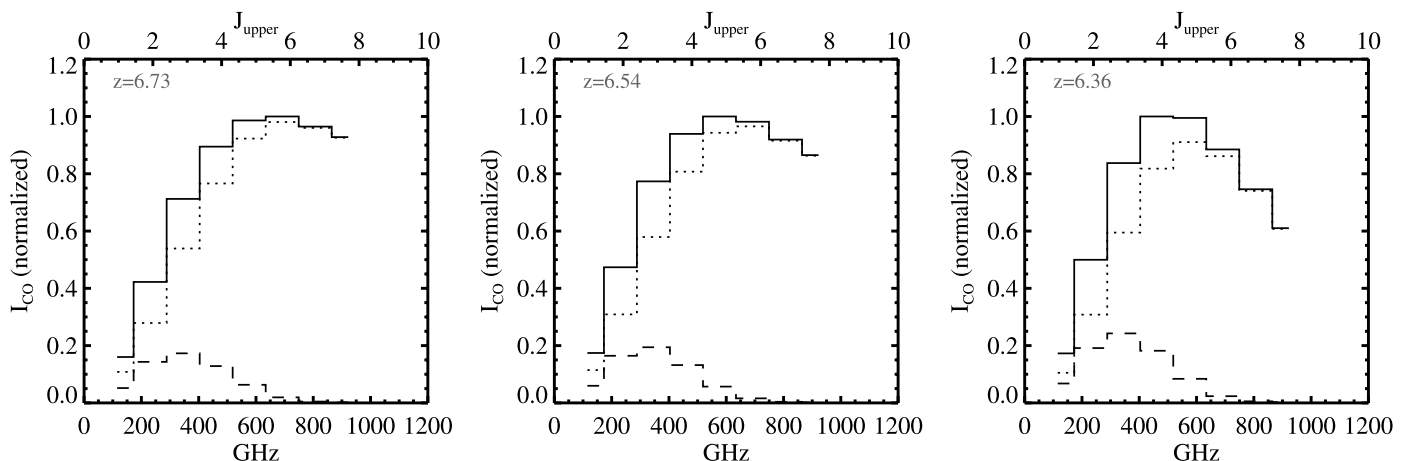

FIG. 2.— CO SED (solid line) at three points during the peak of the quasar phase of our most massive simulated galaxy ($M \sim 10^{13}\ M_\odot$; model Q1). Massive starbursts and dense conditions in the central kiloparsec cause the CO flux density to peak at $J = 8$ prior to and at the beginning of the quasar phase (not shown). During the bulk of the quasar phase, the CO SED peak drops to $J = 6$ owing to quenching of the starburst by black hole feedback and remains roughly constant for the remainder of the quasar's life. As the central AGN quenches the nuclear starburst, less gas is in highly excited ($J \gtrsim 6$) states, and the slope on the blue end of the peak becomes much steeper. The dotted line is the CO SED from just the central kpc, and the dashed line is the contribution from radius = 1–4 kpc). The upper level of each transition is listed on the top axis.
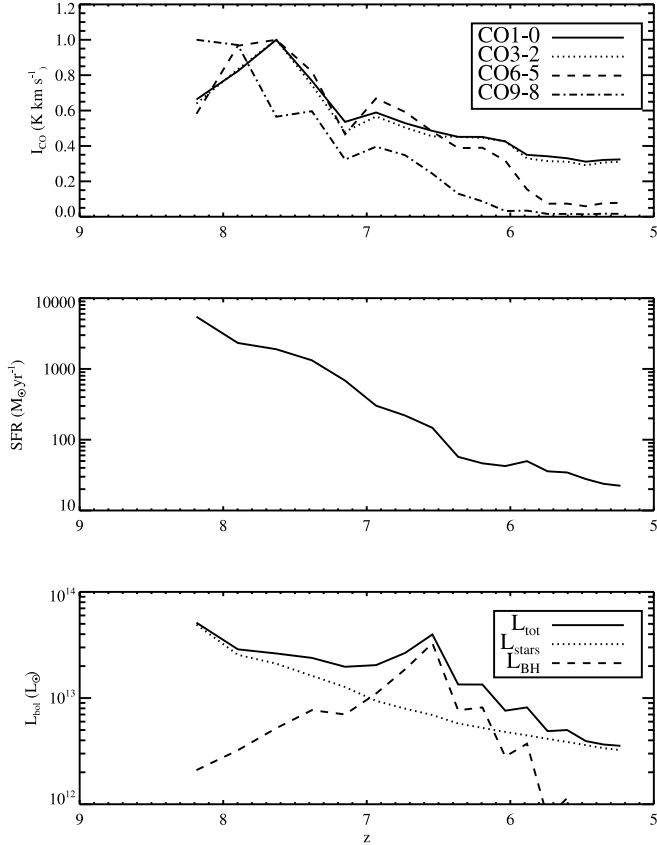
Fig. 3.—*Top*: Velocity-integrated CO intensity (K km s^{-1}) as a function of redshift for various CO transitions for quasar Q1. Each transition is normalized. *Middle*: Star formation rate as a function of redshift. *Bottom*: Quasar bolometric luminosity as a function of redshift. The bolometric luminosity is broken up into contributions by stars and black holes. The bright CO emission in high-*J* transitions during the quasar phase is representative of massive star formation, through the bulk of the spheroid formed during the hierarchical buildup of the quasar host galaxy, prior to the active quasar phase.

again focused on the most massive simulation (Q1), although the results are generic for each of the models studied here. In Figure 4 we show the evolution of the central 2 kpc of the CO($J = 1-0$) emission in the most massive halo, Q1, during the hierarchical buildup of the host galaxy and quasar phase. Individual concentrations in the molecular gas density which have not fully coalesced appear during the buildup of the quasar host galaxy and through parts of the quasar phase (e.g., $z = 6.73$, Fig. 4), giving rise to multiple CO($J = 1-0$) emission peaks. Near the end of the quasar's lifetime, the molecular gas settles into a nuclear disk, with the densest gas in the central ∼500 pc.

The morphological features of our simulated quasar agree reasonably well with observations. Observations of J1148+5251 have revealed two CO($J = 3-2$) emission peaks in the central 2 kpc (Walter et al. 2004), similar to the multiple surface CO surface brightness peaks seen at many points in our models (e.g., Fig. 4). This suggests that the observed multiple surface brightness peaks in the CO morphology of J1148+5251 may owe to separated peaks of high-density emission in the nucleus that have not yet coalesced. To further illustrate this point, in Figure 5 we have plotted the CO($J = 3-2$) emission contours at $z = 6.73$ over three orthogonal viewing angles and six random ones. Most viewing angles exhibit two surface brightness peaks, suggesting that a merger origin for the formation of J1148+5251 is viable.

Within the constraints of our numerical simulations, multiple density peaks in the cold gas appear to be the most plausible ex-

planation for the observed morphology of J1148+5251. Multiple emission peaks in the CO morphology of galaxy mergers have also been noted to arise from large entrainments of molecular clouds in AGN-driven winds (Narayanan et al. 2006b). In the current simulations, however, the characteristic outflow morphologies of Narayanan et al. are not seen during the active quasar phase. Emission from the nuclei of progenitor galaxies can additionally cause multiple CO surface brightness peaks. However, by the time the simulated host galaxy reaches the height of the quasar phase, the most massive nuclei have all merged into the central potential (Li et al. 2007).

The excitation characteristics in the vicinity of massive starbursts can cause transition-dependent CO morphologies. In Figure 6 we show the CO($J = 1-0$), ($J = 3-2$), and ($J = 6-5$) emission contours for the central 2 kpc of the most massive host during the quasar phase. The multiple emission peaks which owe to merging clumps of dense gas ($z = 6.73$ in this plot) appear in all transitions. When the cold gas has coalesced in the nucleus, emission from the lowest excitation gas traced by CO($J = 1-0$) exhibits discrete pockets of emission, whereas higher lying emission originating from denser gas is centrally concentrated. As seen in Figure 2, the warm and dense conditions in the starbursting nucleus of the quasar ensure that the CO remains excited, with the peak flux density at $J = 5-8$. The CO gas in the nucleus is typically excited out of the $J = 1$ level, resulting in discrete pockets of emission in the circumnuclear molecular gas. The higher lying emission, which originates in the warmer, denser cores of GMCs, is more prevalent in the central 500 pc of the quasar, resulting in a smoother distribution.

Owing to the violent nature of the quasar's formation process, the spatial extent of the CO emission has a large dynamic range and varies from ∼2 kpc to ∼300 pc (half-light radius) throughout the evolution of the host galaxy. The more extended morphologies are representative of times when gas is falling into the central potential and in the postquasar phase when winds have produced an extended morphology. More compact CO emission is seen primarily when the cold gas has completely coalesced and the quasar is most active.

The starburst is centrally concentrated in the central ∼250 pc of the quasar host galaxy during the majority of the simulation presented here. Conversely, the CO morphology is not always so compact. The CO emission through $J = 10$ is extended during the buildup of the host galaxy (prior to the quasar phase) owing to merging gas clumps. This implies that CO may not always serve as an adequate tracer of the starburst during the major merger phase of the quasar's formation. During the active quasar phase, when most of the gas has fallen into the nucleus, emission from higher CO transitions (e.g., $J \gtrsim 6$) tends to become compact and faithfully trace the active starburst.

5. CO EMISSION LINES

The simulated properties of the CO emission lines show variations among the models presented in Table 1. In this section we discuss the CO emission lines in terms of the CO($J = 6-5$) lines as the CO SED peaks near $J = 6$ for most of the quasar phase, and thus, this transition best traces the properties of the bulk of the molecular gas. Unless otherwise specified, the nature of the CO line profile as described in the remainder of this section is not seen to vary significantly with the observed transition.

5.1. General Nature of Modeled Line Profiles

In Figure 7 we show a sample of three random CO($J = 6-5$) emission lines from the simulated quasars Q1, Q2, and Q3 at the peak of their respective quasar phases. The first noteworthy

T_B (K km s^{-1})
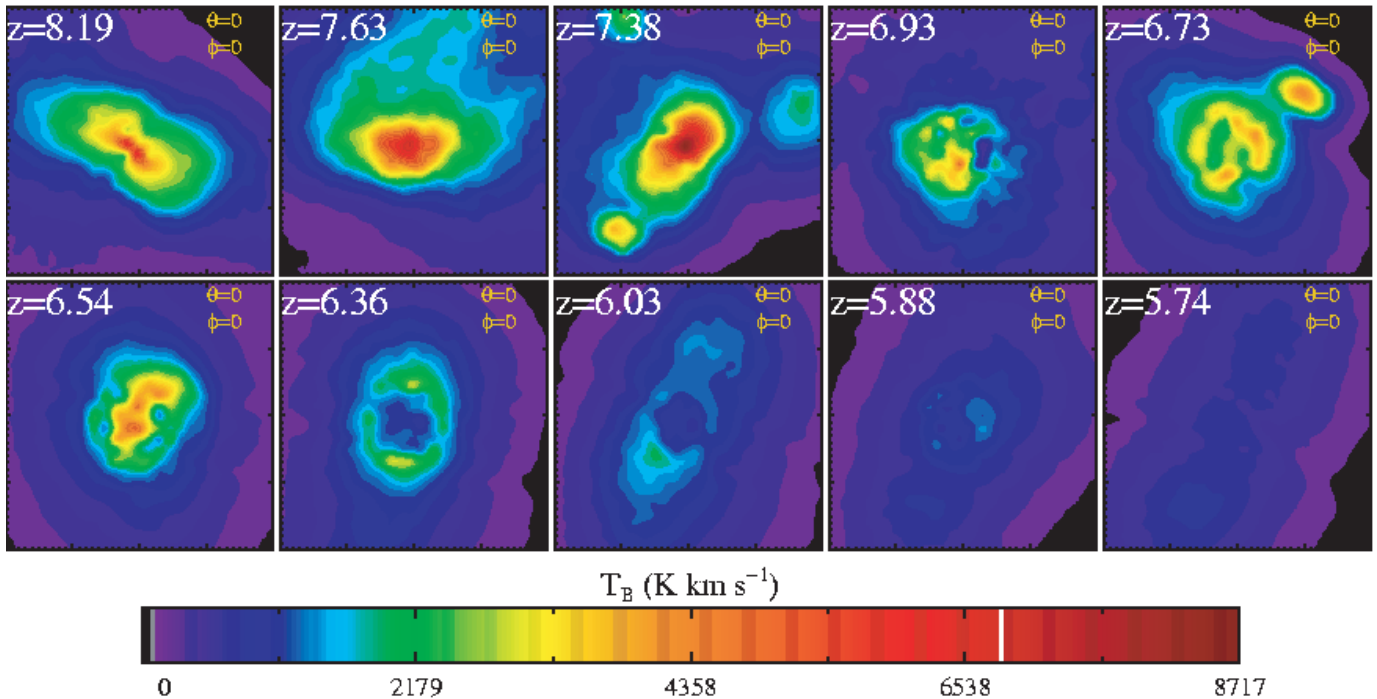
0   2179   4358   6538   8717

FIG. 4.—Evolution of CO($J = 1-0$) emission contours from $z = 8.2$–5.7 in most massive halo, model Q1 ($M \sim 10^{13} \, M_\odot$). Multiple emission peaks are visible as cold gas falls in toward the nucleus, similar to observations of J1148+5251. As the starburst and quasar activity subsides, the CO intensity fades. Each panel is four kpc on a side. The emission is in terms of velocity-integrated intensity (K km s^{-1}), and the scale is at the bottom. The viewing angle of each panel is listed in the top right corner and is always $\theta = 0$, $\phi = 0$ for this figure.

point regarding the CO emission lines from the $z \sim 6$ quasar models is that they are characteristically featured, with a significant amount of substructure. Along many lines of sight, several smaller emission spikes (with $\sigma \sim 50$–100 km s^{-1}) originating in dense CO clumps in the central 2 kpc sit superposed on the broader emission line. These emitting clumps are centrally concentrated in the quasar, and similar emission features are seen in higher spatial resolution spectra.

Another clear feature of Figure 7 is the apparent trend of narrowing line width with decreasing halo circular velocity. The CO line widths are reflective of the circular velocity and are thus strongly dependent on the mass of the quasar host galaxy. To further illustrate this, in Figure 8 we show the mean sight line–averaged CO($J = 6-5$) line width during the hierarchical buildup and quasar phase of the quasars formed in the halos of Q1–Q3. We additionally show the range of sight line–dependent observed line width values. The multiple mergers involved in the formation of the simulated $z \sim 6$ quasars give rise to large velocity dispersions along a number of sight lines during the buildup of the quasar host galaxies. During this time, much of the molecular gas is not virialized, and thus, the typical line widths exhibited represent about twice the expected circular velocity at the spatial extents of the molecular gas. In the quasar phase, as the gas virializes into a molecular disk, the CO line widths drop to values more consistent with the virial velocity of the host. In the most massive ($\sim 10^{13} \, M_\odot$, model Q1; Table 1) halo, this is manifested in broad ($\langle \sigma \rangle \sim 500$–$800$ km s^{-1}) predicted CO emission line widths, whereas in the halos with lower circular velocity (quasars Q2 and Q3), the mean CO line width is ~ 450 and ~ 300 km s^{-1}, respectively. It is important to note that in all cases, while the aforementioned trends hold, a large range of line widths is permitted at all points, as they are strongly sight line–dependent. Another way to view this is through the detailed distribution of

line widths themselves. In Figure 9 we show a histogram of the sight line–dependent line widths during the quasar phase for models Q1–Q3.

These derived line widths are a natural consequence of our initial assumptions of quasar formation in massive halos and that half the cold gas mass is in the molecular phase. Within the confines of our initial assumptions, these results are consistent with virial arguments. Thus, for example, the broad emission lines seen in the massive $\sim 10^{13} \, M_\odot$ halo simply reflect the virial velocity of the host galaxy at the radial extent of the molecular gas distribution, which is of order ~ 550 km s^{-1}.

CO line measurements of J1148+5251 by Bertoldi et al. (2003b) and Walter et al. (2003, 2004) showed CO($J = 3-2$, $J = 6-5$, and $J = 7-6$) emission lines with width $\sim 280 \pm 140$ km s^{-1} (FWHM; corresponding to $\sigma \sim 120 \pm 60$ km s^{-1} for a Gaussian line). While this is a factor of 2–5 narrower than the median line width predicted in our models (Figs. 8 and 9), it is worthwhile to note the nonnegligible fraction of sight lines for each of the quasar models that are compatible with the narrow observed line widths (Fig. 9). Through the quasar phase and the beginning of post-quasar phase, ~ 2–3% of sight lines in the most massive quasar host (Q1) have line widths compatible with the line widths measured in J1148+5251 (Bertoldi et al. 2003b; Walter et al. 2003, 2004). The smaller virial velocity of the lower mass halos (Q2 and Q3) naturally produce more sight lines with narrow line widths compatible with observations. During the quasar phase, the quasar formed in the $4 \times 10^{12} \, M_\odot$ halo (model Q2) shows CO($J = 6-5$) emission line widths consistent with observations $\sim 5\%$ of the time, and the quasar formed in the $1.5 \times 10^{12} \, M_\odot$ halo (model Q3) reveals CO($J = 6-5$) line widths consistent with observations $\sim 10\%$ of the time.

In an effort to understand the relationship of these models to the measured CO line width of J1148+5251, it is of interest to
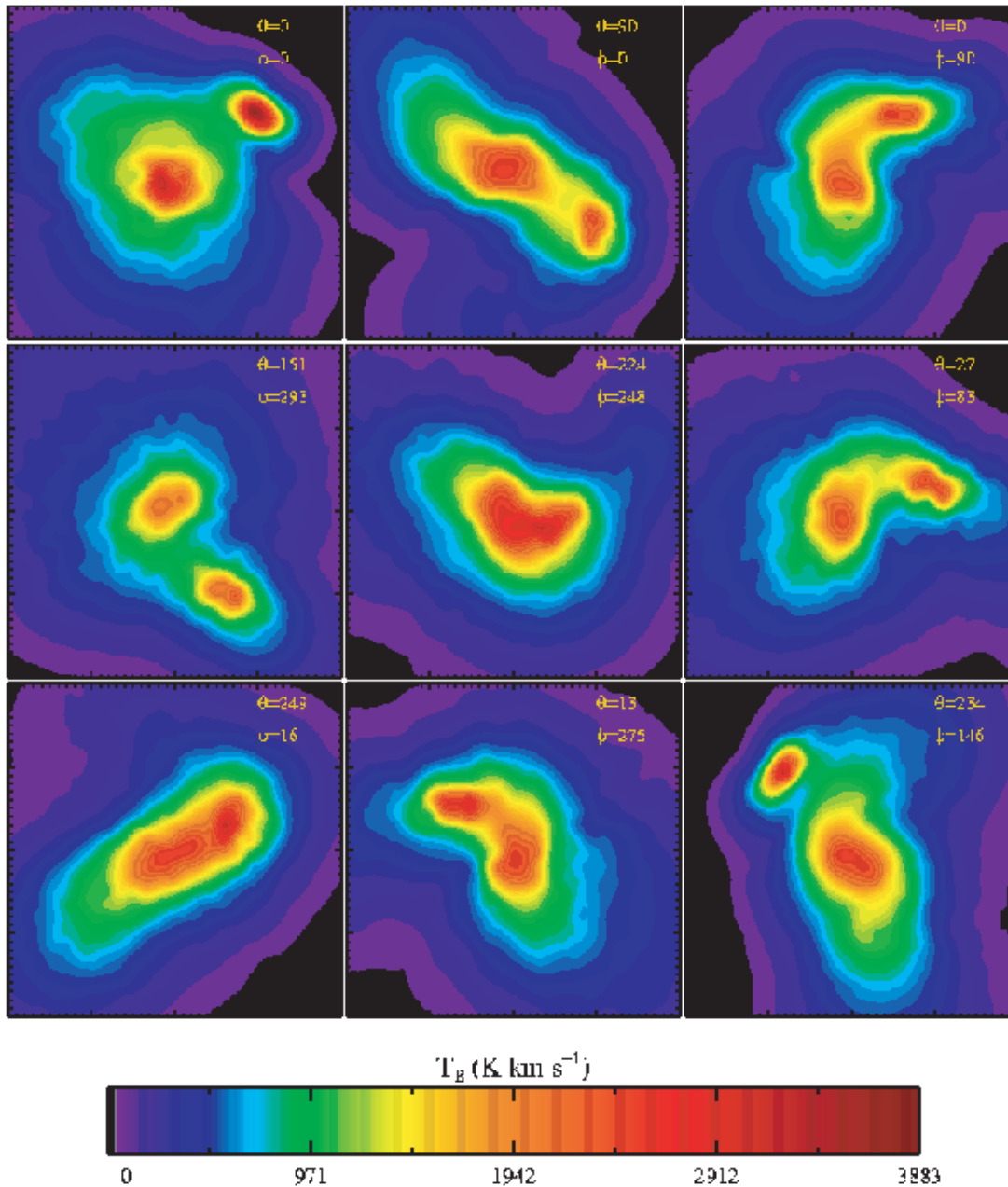
Fig. 5.—CO($J = 3$–2) emission from most massive quasar host (Q1) at $z = 6.73$, while cold gas from the merger is still infalling. Top three panels are three orthogonal viewing angles, and the bottom six viewing angles are randomly drawn. The orientation for the line of sight is in the top right corner of each panel. Along many different viewing angles, multiple CO components are visible, similar to the observed morphology of J1148+5251 (Walter et al. 2003), indicating a viable merger origin for J1148+5251. Each panel is four kpc on a side. The emission is in terms of velocity-integrated intensity (K-km s^{-1}), and the scale is at the bottom.

explore the origin behind the particular percentages of sight lines that are compatible with observations, and possible trends which may tend observations toward particular sight lines. We thus focus the remainder of this section on this investigation. We conclude the section with a discussion as to what circumstances may bring agreement between our simulations and observations and the implications of these results with respect to potential observable tests motivated by these models.

5.2. Effect of Merger Remnant Structure and Disk Formation on Line Widths

We have thus far considered the formation of quasars hierarchically through multiple mergers whose physical conditions were derived self-consistently from cosmological simulations. It is possible that not all quasars at $z \sim 6$ form via numerous violent merging events, but rather through a more ''ordered'' merger. It is thus worth quantifying the potential dependence of line width on merger history, and in particular, how a more ordered merger remnant may affect the observed line widths. To provide a limiting example, we have conducted a test simulation of a coplanar binary merger in a halo of $\sim 10^{13}$ $M_{\odot}$ (model Q4; Table 1). The progenitors were initialized with a Hernquist (1990) profile, spin parameter $\lambda = 0.033$, and circular velocity $V_{200} \sim 600$ km s^{-1}. The disks had an initial gas fraction of 0.99, and the virial properties were scaled to be appropriate for $z = 6$ (Robertson et al. 2006c).
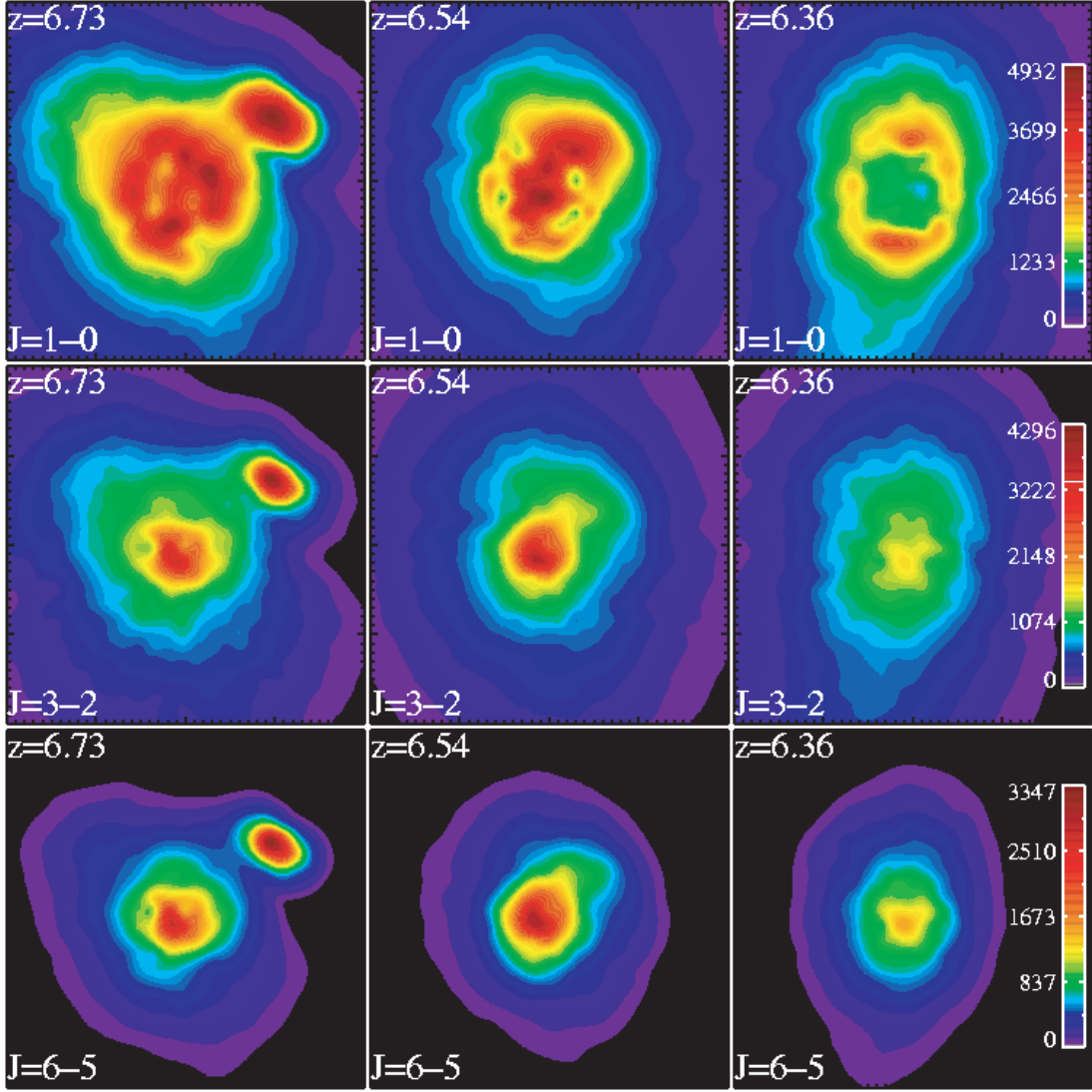
FIG. 6.—Excitation-dependent CO morphologies: CO($J = 1-0$), ($J = 3-2$), and ($J = 6-5$) emission contours from most massive quasar host (Q1) during the peak of the quasar phase. Columns are constant in redshift, and rows are constant in transition. Multiple CO emission peaks are seen arising from merging cold clumps of gas, as well as circumnuclear gas in the ($J = 1-0$) case. The gas in the central $\sim$kpc is highly excited and, thus, does not show prominent ($J = 1-0$) emission, but causes the ($J = 3-2$) and ($J = 6-5$) emission to be centrally concentrated. Multiple CO emission peaks are seen in higher lying transitions owing only to merging gas, as the bulk of the gas in the central $\sim$kpc is highly excited. These results are robust across all modeled viewing angles. The viewing angle for each panel is the same and is $\theta = 0$, $\phi = 0$, for comparison with Figs. 4 and 5. Each panel is four kpc on a side, and each row (transition) is on its own scale to facilitate interpretation. The scales are on the right, and the units are in terms of velocity-integrated Rayleigh-Jeans temperature (K-km s^{-1}).

In Figure 10 we show the CO($J = 3-2$) morphology for the resultant quasar over two orthogonal viewing angles and their corresponding unresolved emission spectra. The remnant forms a strong disklike morphology, consistent with the findings of Robertson et al. (2006a) and Springel & Hernquist (2005). As expected, the CO line width and profile is a sharp function of the viewing angle of the disk. Averaged over 250 random sight lines, we find that the predicted CO($J = 6-5$) emission line width from this source is consistent with the observed line width J1148+5251 $\sim$4% of the time, comparable to the more massive quasar hosts (Q1 and Q2) which formed from multiple mergers.

The percentage of sight lines compatible with observations in the binary merger Q4 arises from a limited range of angles a disk can be from face-on to keep line widths within a particular limit. Specifically, if one considers an inclined toy disk of pure gas with velocity dispersion σ_{vir}, then in order for observed velocity dis-

persions to fall below a particular value, σ_{obs}, the inclination angle from face-on is limited by

$$\theta < \sin^{-1}\left(\frac{\sigma_{\mathrm{obs}}}{\sigma_{\mathrm{vir}}}\right). \qquad (2)$$

However, inclinations along both the polar (θ) and azimuthal (ϕ) axes have to be within this limit of a face-on configuration to keep the line-of-sight velocity dispersion below observed line widths. As such, the probability of having both θ and ϕ randomly drawn such that they both fall below a critical value to match an observed line width is

$$P(\theta < \theta_{\mathrm{crit}}, \phi < \phi_{\mathrm{crit}}) = \frac{4}{\pi^2}\left[\sin^{-1}\left(\frac{\sigma_{\mathrm{obs}}}{\sigma_{\mathrm{vir}}}\right)\right]^2, \qquad (3)$$
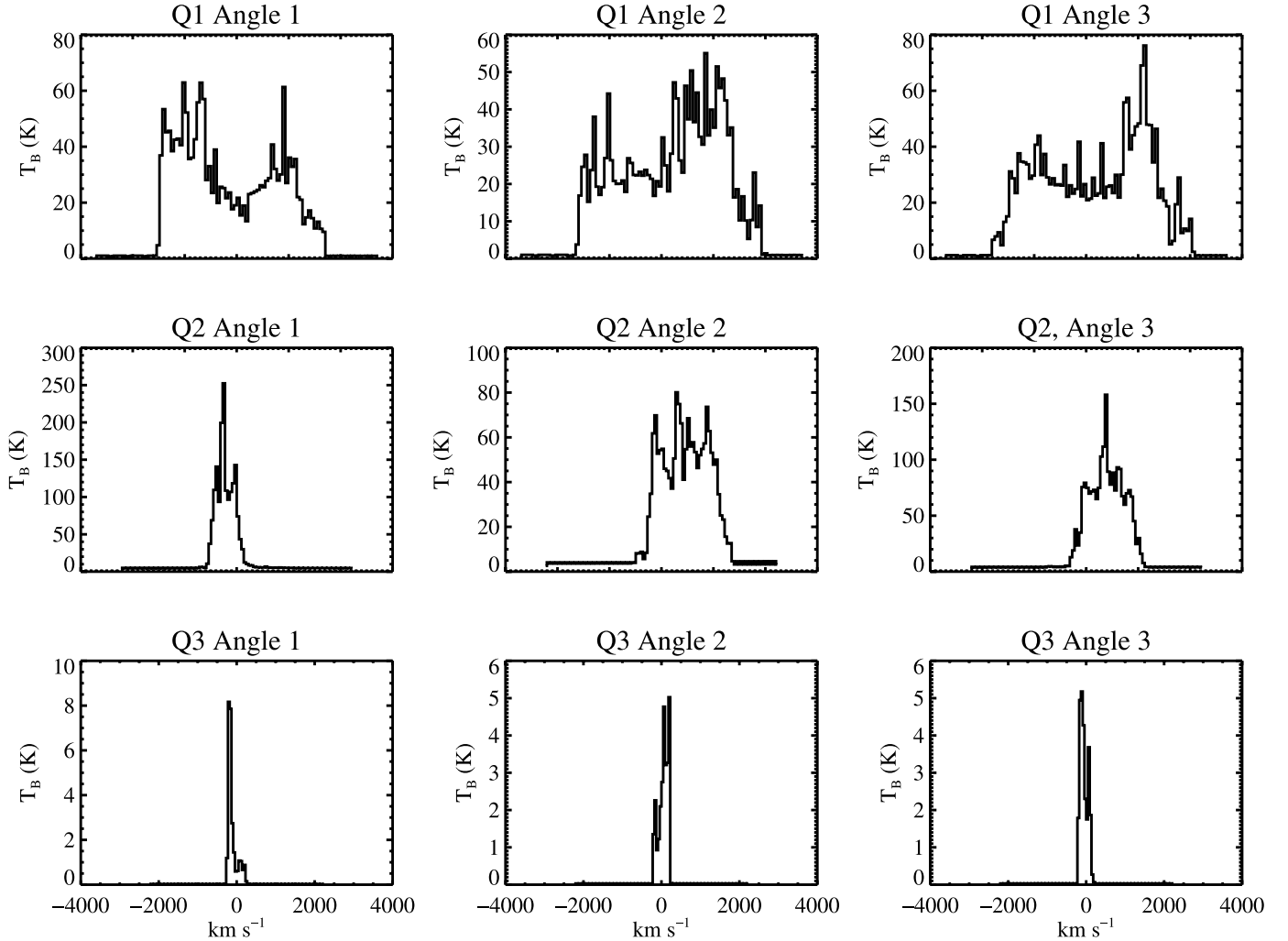
Fig. 7.—CO($J = 6-5$) emission lines from model quasars Q1, Q2, and Q3 at peak of their quasar phases viewed from three random sight lines. The first row corresponds to quasar Q1, the second to Q2, and the third row to Q3. The characteristic emission line widths drop with halo mass, although they remain featured in each model with several substructure spikes superposed on broader lines. Spectra have been convolved with a circular 5″ Gaussian beam and modeled at an angular diameter distance of 1 Gpc.

where $P \approx 4\%$ for $\sigma_{obs} = 180$ km s^{-1} (the upper limit σ of the observed line in J1148+5251), and $\sigma_{vir} = 600$ km s^{-1}. This probability then represents the upper limit of the fraction of sight lines that will be compatible with the observed CO line width in J1148+5251 for disks with circular velocity $\sim$500 km s^{-1}.

This clarifies why the percentage of sight lines compatible with observations in the massive multiple-merger models (Q1–Q3) is relatively small. The cold gas in the three quasars which formed out of multiple nonidealized mergers (Q1–Q3) settles into rotating nuclear disks. As an aside, it is interesting to note that the amount of rotationally supported gas is seen to be dependent on the mass of the galaxy. Namely, the lower mass halos show a larger percentage of gas in stable rotation. To illustrate this, in Figure 11 we show the fraction of rotationally supported gas for quasars Q1–Q3 as a function of redshift, noting in particular the points of peak quasar activity. When the most massive galaxy (Q1) is seen as a quasar, roughly 50% of the H$_2$ gas is rotationally supported. Conversely, in the lowest mass model (Q3), $\sim$90% of the gas is rotationally supported. This may be a direct result of the amount of energy input from the central quasar during these times. Cox et al. (2007) demonstrated that the amount of rotationally supported gas in galaxy mergers decreases with increasingly efficient winds. During the peak of the quasar phase, the black hole

luminosity is over an order of magnitude brighter in model Q1 than in Q3.

In either case, however, large percentages of the gas in all of the quasars (Q1–Q3) are seen to be rotationally supported during the quasar phase. Because of this, the number of sight lines compatible with observations is roughly characterized by equation (3). Thus, the most massive model (Q1) shows line widths compatible with observations $\sim$2–3% of the time, consistent with a predicted upper limit of $\sim$4% for $\sim$10^{13} $M_{\odot}$ halos. Similarly, in the lowest mass model (Q3), where $\sim$90% of the gas is rotationally supported, the 10% of sight lines seen to be compatible with observed line widths is compatible with the predicted upper limit of $\sim$13%. The fact that the modeled fraction of sight lines is always slightly smaller than the toy model in equation (3) owes to the fact that some of the gas in the galaxy is still highly dynamical and not virialized.

5.3. CO *Line Width–Quasar Luminosity Relation: Potential Selection Effects*

Given the dispersion of CO($J = 6-5$) line widths along different lines of sight, an interesting relation to explore is one between the optical quasar luminosity and CO emission line width in search of potential observational selection effects which may tend
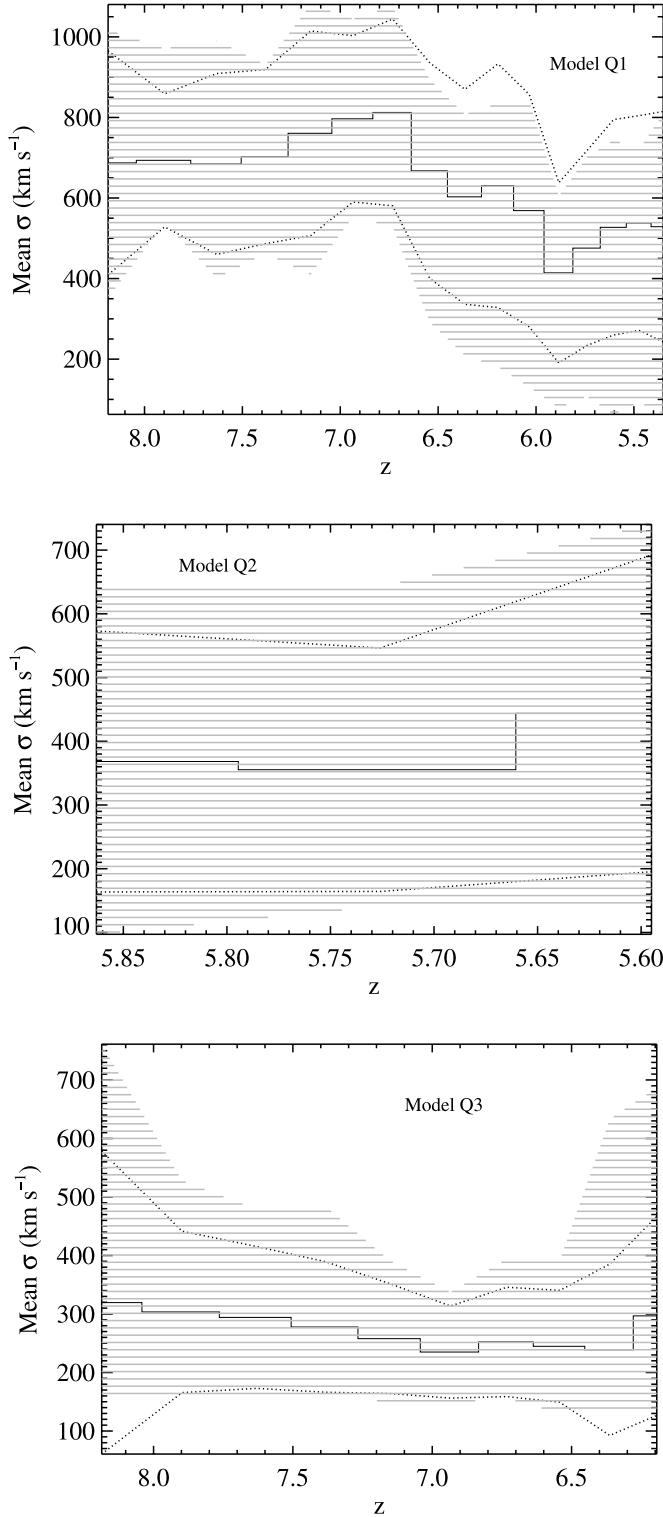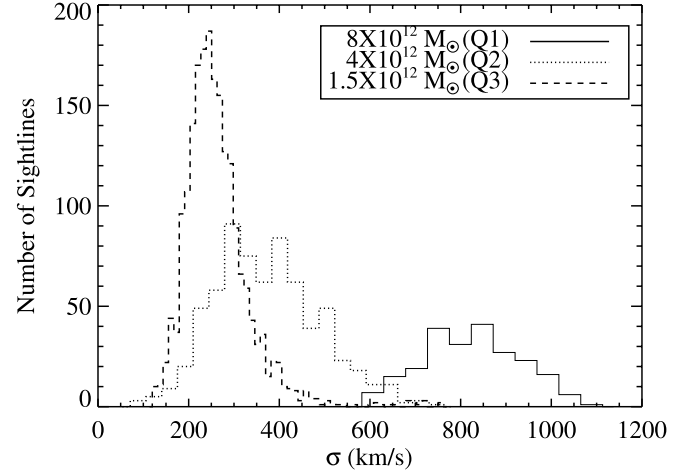
Fig. 9.—Histogram of sight line–dependent line widths during quasar phase for three halo mass models. The mean line width traces the virial velocity of the host galaxy and, thus, becomes narrower in lower mass galaxies. In all cases, a broad range in line widths is observable.

observations of $z \sim 6$ quasars toward smaller line widths. In Figure 12 we plot the σ from the CO($J = 6$–5) line width as a function of the attenuated rest-frame B-band luminosity over 5000 lines of sight throughout the quasar phase for the most massive model, Q1. We utilize the methodology of Hopkins et al. (2005d) in computing the dust-attenuated quasar luminosity and include contributions from both the stellar component and the central AGN.

There is a general trend for sight lines which show the brightest rest-frame B-band luminosity to have smaller CO line widths. This can be understood via decomposition of the quasar luminosity into its stellar and AGN components. Specifically, while
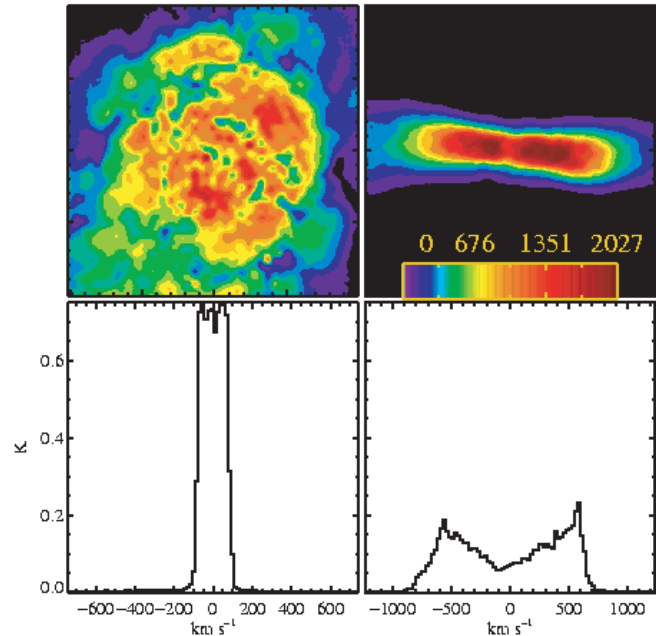

Fig. 8.—Sight line–averaged velocity dispersion (σ) of CO($J = 6$–5) emission lines (*solid line, middle*) as a function of redshift for quasar models Q1–Q3. The shaded area shows the range of derived σ over 250 randomly sampled sight lines, and the upper and lower dotted lines show the 2 σ line widths for each snapshot. The spectra have been convolved with a circular 5″ Gaussian beam and binned to 50 km s^{-1}. During the hierarchical buildup of the host galaxy, the H$_2$ gas is highly dynamical, and the typical line widths are broader than the virial velocity of the host galaxy by a factor of $\sim$1.5–2. As the gas virializes during the quasar phase, the line widths drop and roughly trace the virial velocity of the galaxy. A range of line widths are permitted throughout the evolution of the host galaxy, with larger numbers of sight lines being compatible with the narrow ($\sigma \sim 120$ km s^{-1}) detected line in J1148+5251 near the end of the quasar phase. The number of sight lines compatible with observations naturally increases in the lower mass halos (Q2 and Q3), as the CO lines faithfully trace the virial velocity of the galaxy during the quasar phase.

Fig. 10.—CO($J = 1$–0) morphology and unresolved line profiles of remnant formed from binary merger simulation (model Q4) across two orthogonal sight lines (face-on and edge-on). The progenitors were initialized on a coplanar orbit in a $\sim 10^{13}$ $M_\odot$ halo. The resultant quasar host galaxy has large rotating molecular disk, resulting in narrow observed emission lines in face-on viewing angles and broad lines in edge-on viewing angles. Approximately 4%–5% of sight lines show narrow line widths compatible with observations of J1148+5251 (see eq. [3]). The maps are 12 kpc across, and the scale is in units of K-km s^{-1}.
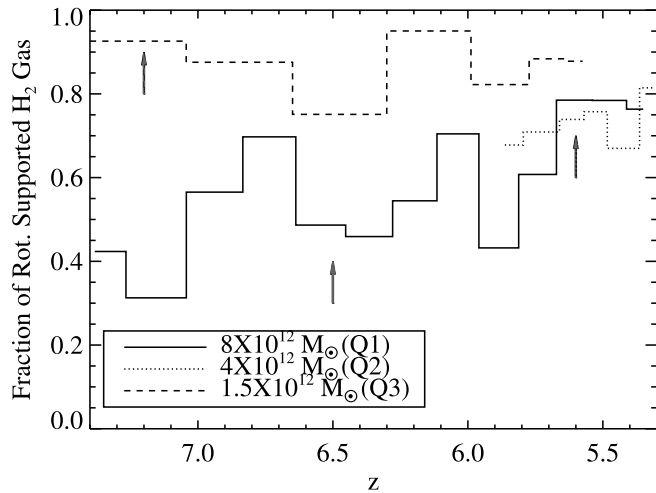
Fig. 11.—Fraction of rotationally supported molecular gas in quasars Q1–Q3. Gas is considered to be in rotational support if its rotational velocity is at least 80% the expected circular velocity at that radius. Arrows point to redshift of peak quasar activity (also listed in Table 1). Gas is seen to more easily settle into a stable rotational configuration in the lower mass quasar hosts, although all quasars naturally form relatively strong disks during the quasar phase.

the stellar luminosity does not vary much with viewing angle, the contribution of the central black hole to the total luminosity is strongly dependent on the viewing angle with respect to the rotating molecular gas. Directions which view the molecular disk in an edge-on configuration result in a heavily obscured central AGN. Along these sight lines, the emergent CO emission line is typically broad (e.g., Fig. 10, *bottom right*). Conversely, when the molecular disk is seen in a more face-on viewing angle (and thus has narrower CO emission lines), the central AGN can be viewed relatively unobscured, and the attenuated rest-frame *B*-band luminosity is consequently higher. This effect is typical during the quasar phase, and only rarely is the black hole relatively unattenuated through an edge-on sight line, which causes broad CO lines to be visible when the rest-frame *B*-band luminosity peaks.
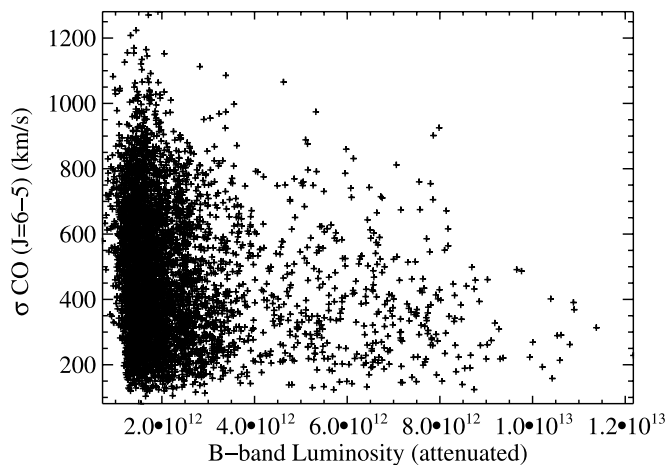

Fig. 12.—CO($J = 6$–5) emission line width (σ) vs. attenuated rest-frame *B*-band luminosity. The brightest quasar luminosities correspond to face-on molecular disk configurations where the central AGN is the least obscured. These face-on sight lines additionally show narrow CO line widths. Thus, surveys which select quasars for optical luminosity may preferentially select objects that have narrow CO line widths. This may have important consequences for using CO as a dynamical mass indicator in quasars.
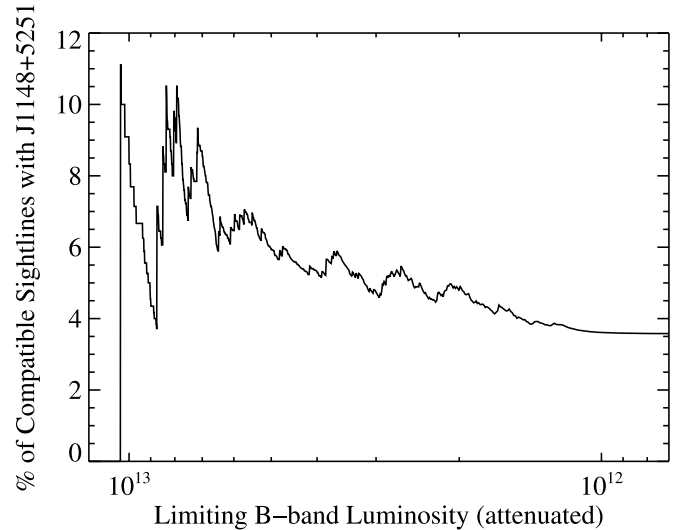

Fig. 13.—Percent of sight lines of $\sim 10^{13}$ $M_\odot$ quasar over which line widths are compatible with observations vs. limiting rest-frame *B*-band luminosity. Natural molecular disk formation in the quasar host galaxy gives rise to a selection effect which enhances the likelihood that flux-limited optical surveys will view the quasar in a face-on configuration. These viewing angles also typically have narrower CO line widths and, thus, may increase the chances of viewing a narrow emission line in quasars which is not necessarily characteristic of the true sight line–averaged mean line width. Line widths are derived from CO($J = 6$–5) line profiles and compared to upper limit of sole CO detection at $z \sim 6$, J1148+5251. Rest-frame *B*-band luminosities are dust attenuated and calculated using the methodology of Hopkins et al. (2005d).

The results of this relationship between bolometric luminosity and line width suggest a potential selection effect which may cause quasars selected for optical luminosity to have systematically lower CO line widths, owing to the preferred face-on viewing angle for the molecular disk. In Figure 13 we plot the percentage of sight lines with line widths compatible with observations as a function of limiting rest-frame *B*-band luminosity. For the highest flux cuts, the fraction of sight lines with narrow line widths increases from 2%–3% to $\sim 10\%$. This selection effect is robust across both the lower mass halo models as well. In models Q2 and Q3, the fraction of sight lines compatible with observations increases to $\sim 15\%$ and 25%, respectively, for the highest luminosity cuts.

Finally, we note that the viewing angles corresponding to the smallest ($2\,\sigma$) line widths in our simulations typically fall within a 25° range in polar and azimuthal angle from face-on. This range of angles is consistent with recent observational studies which have suggested that the commonly observed narrow CO line widths of high-z quasars may correspond to a preferred viewing angle of 10°–15° from face-on (Carilli & Wang 2006; Wu 2007).

5.4. Interpretation of $z \sim 6$ Quasar Observations

Our simulations show that $z \sim 6$ quasars which form in massive halos will characteristically have broad mean line widths, consistent with simple virial arguments. The mean simulated line widths are in apparent contradiction to observed narrow ($\sigma \sim 120 \pm 60$ km s^{-1}) line widths of the sole CO detection at $z \sim 6$ (Walter et al. 2004), although a nonnegligible fraction of sight lines (ranging from 2%–3% for the most massive model to $\sim 10\%$ in the lowest mass model) are compatible with this observation. Potential selection effects owing to molecular disk formation in these galaxies will increase the probability of narrow-line detection when selecting quasars for optical luminosity, ranging from $\sim 10\%$ in the most massive quasar host to 25% in less

massive ones. The full dispersion in line widths is predicted to become more apparent at lower optical luminosities (Fig. 12).

Our models find that quasars which form in the lower end of our halo mass range at $z \sim 6$ (e.g., quasars Q2 and Q3) may have similar rates of detection as those which form in the most massive $\sim 10^{13} M_\odot$ halos (e.g., quasar Q1). This owes to the competing effects of smaller quasar lifetimes in the lower mass halos, along with the existense of more lower mass halos in the simulated cosmological volume. Specifically, the quasars formed in the $4 \times 10^{12} (1.5 \times 10^{12}) M_\odot$ halos have luminosities $\gtrsim 10^{13} L_\odot$ for a factor of ~ 2.5 (14) less time than the quasar formed in the $10^{13} M_\odot$ halo (Table 1). However, standard halo mass functions predict more low-mass halos than massive $\sim 10^{13} M_\odot$ halos (Press & Schechter 1974; Sheth & Tormen 2002; Springel et al. 2005). The cosmological simulations of Li et al. (2007; which were used in this work) found approximately 3 (7) times as many halos of mass $5 \times 10^{12} (2 \times 10^{12}) M_\odot$ compared to the single $\sim 10^{13} M_\odot$ halo identified in the simulation box at $z \sim 6$ (Li et al. 2007; Fig. 14). In this sense, quasars which form in lower mass halos may be identified at similar rates as those which form in $\sim 10^{13} M_\odot$ halos.

One result of this work is to motivate observational tests of these models. A direct prediction of these simulations is that a CO survey from a large sample of quasars at $z \sim 6$ which probes lower on the optical luminosity function may directly constrain the range of potential line widths which originate from high-redshift quasars. At the median rest-frame B-band luminosity, our models predict that a large range of line widths should be observed (Fig. 12). A potential caution associated with this test is that physical processes on scales below the resolution of our simulations may limit optical detections of quasars with edge-on disks at $z \sim 6$. For example, if a dusty molecular torus exists on scales smaller than ~ 100 pc and provides high levels of obscuration along sight lines other than face-on, then the variation of optical luminosity with inclination angle will be steeper than suggested by Figure 12. It is thus not a straightforward assumption that optical surveys will need to probe only an order of magnitude lower in rest-frame B-band luminosity to test these models as Figure 12 suggests, but rather it is in the limit that quasars with relatively inclined disks at $z \sim 6$ can be detected that these models predict a broad range of CO line widths at lower optical luminosities.

A more clear test may come from observations of the progenitors of $z \sim 6$ quasars themselves. For example, a direct prediction from these models is that CO observations of either the most massive progenitor galaxies prior to the merger (e.g., at $z \sim 8$; see Table 1 of Li et al. 2007) or the ongoing mergers themselves may exhibit a large dispersion in CO line widths, with median velocity dispersion reflective of the halo virial velocity (Fig. 8). The identification of potential progenitors at $z \gtrsim 7$ is predicted to be feasible through z-band dropouts (Robertson et al. 2007).

In either case, these models suggest that surveys at $z \sim 6$ which observe either the most massive progenitors of quasar host galaxies or highly inclined disks (closer to edge-on and likely lower luminosity) associated with $z \sim 6$ quasars will see a broader dispersion of CO line widths. The model halos presented here reflect the range of halo masses in our cosmological simulation which were feasibly able to create a $z \sim 6$ quasar. As such, based on the line widths seen in our lowest mass host galaxy (Q3), samples of CO detections at $z \sim 6$ which probe quasars with a range of disk inclination angles should find a median line width at least $\sim$twice the value of the sole detection. Surveys which observe quasars with inclined molecular disks and still find consistently narrow line widths may reflect an inability of our radiative transfer simulations to fully capture the appropriate physics
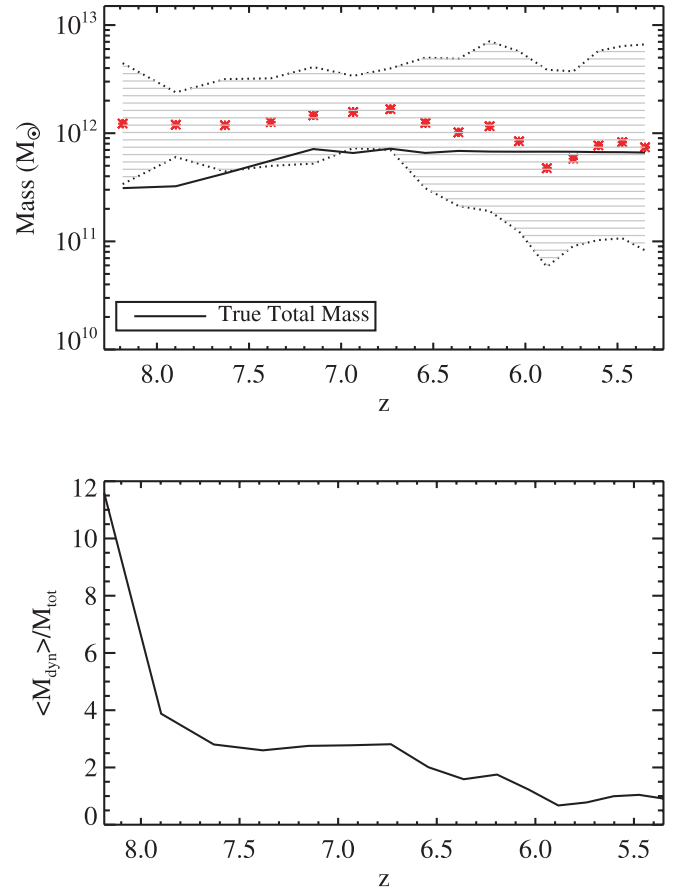

Fig. 14.—*Top*: Median dynamical masses derived from line widths over 250 random sight lines through the hierarchical buildup and evolution of quasar host galaxy (*red crosses*). The shaded region represents the 3 σ range of sight line–dependent derived dynamical masses, and the solid line represents the true total mass within the central 2 kpc. The dynamical masses are derived assuming an inclination angle of $30°$ and a molecular spatial extent of 2 kpc. *Bottom*: Ratio of median derived dynamical mass to total mass. During the hierarchical buildup and early quasar phase, much of the gas is highly dynamical; consequently, derived dynamical masses from CO line widths do a poor job representing the true enclosed mass, typically overestimating by factors of 2–5. As the gas virializes, the sight line–averaged CO line width is a better estimator of the dynamical mass. A large range of values is permitted, consistent with the spread in CO line widths seen in Fig. 8.

necessary to predict accurate CO line widths form these early-universe galaxies. If, for example, our assumptions regarding molecular gas content or CO abundances are incorrect, it could be that CO emission is preferentially seen in lower velocity gas in the host galaxy. Alternative possibilities may include super-Eddington accretion for the central black hole which may allow for luminous quasars at $z \sim 6$ in less massive halos than those adopted here (e.g., Volonteri & Rees 2005). It is, however, attractive that the simulations presented here do provide a model for the CO emission from the earliest quasars which are consistent with observations of the CO excitation and morphology of J1148+5251. More observations to fully determine the nature of CO line widths in $z \sim 6$ quasars will be necessary to assess the validity of this aspect of our modeling.

6. SPHEROID, BLACK HOLE, AND DYNAMICAL MASS

Because submillimeter-wave radiation typically does not suffer the heavy extinction characteristic of optical emission, CO lines are often used as dynamical mass indicators in dusty starburst galaxies. Dynamical masses are derived assuming that the emitting gas is rotationally supported and that the line width provides a

measure of the rotational velocity. Here we assess the usage of CO-derived dynamical masses in $z \sim 6$ quasars. As a case study, we focus on the most massive simulation ($\sim 10^{13}\ M_\odot$; model Q1), although the trends are generic for all quasars presented in this work.

Generally, theoretical arguments have predicted that the M_{BH}-σ_v and M_{BH}-M_{bul} relations show only weak evolution with redshift (Robertson et al. 2006c). Using numerical simulations of galaxy mergers by Cox et al. (2006b) and Robertson et al. (2006c) that include black hole feedback, Hopkins et al. (2007c) found that the normalization of the M_{BH}-M_{bul} relation shows weak (~ 0.3–0.5 dex) trends toward larger M_{BH}/M_{bul} from $z = 0$ to 6. The simulations presented here provide additional support for a scenario in which the stellar bulge and central black hole grow coevally in the earliest galaxies.

In the most massive galaxy presented here, the supermassive black hole grows rapidly during the hierarchical buildup of the quasar host galaxy and reaches a total mass of $\sim 2 \times 10^9\ M_\odot$ during the peak quasar phase, similar to black hole mass estimates in J1148+5251 (Willott et al. 2003). Owing to the extreme star formation rates which can be as large as $\sim 10^4\ M_\odot\ yr^{-1}$ between redshifts $z = 9$ and 8 during the final violent mergers (e.g, Fig. 3), the bulge reaches a total mass of $\sim 10^{12}\ M_\odot$ by the quasar phase. The black hole and stellar bulge masses are related such that $M_{BH} = 0.002 M_{bul}$ during the quasar phase, roughly consistent with the local M_{BH}-M_{bul} relation (Li et al. 2007; Magorrian et al. 1998; Marconi & Hunt 2003). We note, however, that during the peak of the quasar activity, the M_{BH}-σ_v relation is not necessarily obeyed, as the stellar bulge is not dynamically relaxed.

The massive starburst at $z \gtrsim 7$ results in an ISM highly enriched with metals, consistent with the observed Fe II/Mg II abundances, [C II] emission, CO emission, and dust masses for $z \sim 6$ quasars (Barth et al. 2003; Bertoldi et al. 2003a; Dietrich et al. 2003a; Freudling et al. 2003; Jiang et al. 2006; Maiolino et al. 2005; Walter et al. 2003, 2004). Li et al. (2007) have found that the metallicity in the simulated $\sim 10^{13}\ M_\odot$ quasar presented here is solar to supersolar during the quasar phase, owing to the $\sim 10^4\ M_\odot\ yr^{-1}$ starburst during the hierarchical merging process of the quasar formation. These findings are consistent with the mean abundances of ~ 4 times solar in a sample of $4 < z < 5$ quasars observed by Dietrich et al. (2003b) and imply that black hole growth and stellar bulge formation are correlated at high redshifts. These simulations support findings that the relationship is regulated by feedback from supermassive black holes (e.g., Di Matteo et al. 2005; Robertson et al. 2006c; Hopkins et al. 2007c).

CO observations of high-z quasars have suggested that central black hole masses may be excessively large compared to the stellar bulge mass as predicted by the present-day M_{BH}-M_{bul} relation. Dynamical mass estimates of J1148+5251 using CO line measurements have indicated that the stellar bulge may be undermassive by a factor of ~ 10–50 if the present-day M_{BH}-M_{bul} relation holds at $z \sim 6$ (Walter et al. 2004). Studies of other quasars at $z \gtrsim 3$ using CO line widths as a proxy for enclosed mass have arrived at similar conclusions (Shields et al. 2006).

In order to investigate the usage of CO as a dynamical mass indicator, in Figure 14 we plot the evolution of the median dynamical mass of the quasar host galaxy from the most massive simulation (Q1) derived from the CO($J = 6$–5) emission line over 250 random lines of sight, as well as 3 σ contours for the observed range of line widths. In particular, we show

$$M_{dyn} = k \frac{\sigma^2 R}{G \sin(i)}, \qquad (4)$$

where we use an adopted k of 8/3 and assume an average inclination angle of $30°$. We plot the total mass of the host galaxy (within the central 2 kpc) throughout its evolution, including the multiphase ISM, dark matter, stars, and black holes. We additionally plot the ratio of the median derived dynamical mass to the total mass enclosed. The dynamical mass is derived from the width of the CO($J = 6$–5) line as the CO excitation peaks at the $J = 6$ level, and this transition thus best traces the bulk of the molecular gas during the quasar phase of our simulated galaxy. We note, however, that the line widths from lower transition lines do not deviate much from these trends.

During the hierarchical buildup of the host galaxy (prequasar phase), the gas is still highly dynamical and not completely virialized. This results in large CO line widths and, consequently, derived dynamical masses which largely overestimate the true mass. During this time, the typical derived dynamical mass results in an overestimate of the true mass by a factor of ~ 2–5. As the gas becomes more rotationally supported during the quasar phase, the CO($J = 6$–5) line width serves as a better tracer of the mass enclosed. These results are consistent with similar derivations by Greve & Sommer-Larsen (2006), who found that CO can serve as an accurate dynamical mass tracer in merger simulations to within 20%.

An important point from Figure 14 is that a large sight line–dependent range of values are possible for derived dynamical masses. While the median line widths provide reasonable estimates of the true mass, many lines of sight permit significant underestimates. The radiative transfer simulations presented here may then bring some resolution between CO observations which are suggestive of a strong evolution in the M_{BH}-M_{bul} relation at high redshift and models which imply a lesser evolution between present epochs and early times. Figure 14 shows that a large range of dynamical masses may be inferred simply based on the observed viewing angle. While the median CO line width accurately traces the enclosed mass for the bulk of the quasar phase, potential selection effects (Figs. 12 and 13) may bias masses derived from CO line widths from quasars toward an underestimate of the true mass. These model results are consistent with the recent study by Wu (2007), who found that CO line widths provided a particularly poor estimate of bulge velocity dispersion for local Seyferts with line widths narrower than $\sim 400\ km\ s^{-1}$ (FWHM; $\sigma \sim 170\ km\ s^{-1}$). In contrast, the inclination-corrected CO line width was found to correspond well with the bulge velocity dispersion.

7. COMPARISONS TO OTHER HIGH-REDSHIFT POPULATIONS

A natural question which arises from this work is, how do the CO properties of these extreme $z \sim 6$ objects relate to other known starburst and AGN populations? Two extreme high-redshift galaxy populations which may serve as interesting comparisons are (1) optically selected quasars and (2) dusty submillimeter selected galaxies at $z \sim 2$ (see respective reviews by Solomon & Vanden Bout 2005 and Blain et al. 2002).

7.1. Quasars

Only a handful of quasars have been detected in molecular line emission owing to beam dilution and limited sensitivity at millimeter and submillimeter wavelengths. As of the writing of the recent review by Solomon & Vanden Bout (2005), there have been about 16 quasars at $z \gtrsim 1$ for which molecular gas emission properties have been published.

Deciphering the molecular gas morphology remains an issue for most quasars, since the majority of them have been detected in molecular line emission with the help of gravitational lensing, resulting in multiple imaging. The spatial extent of the molecular emission in most quasars appears to range from ~ 1 to 5 kpc (Solomon & Vanden Bout 2005), similar to the simulations presented here as well as observations of J1148+5251. Multiple CO emission peaks are detected less often, although it is not clear whether or not this is a spatial resolution issue. Of seven imaged quasars listed in the recent review by Solomon & Vanden Bout (2005), three have clear CO companions (including J1148+5251), with distances in the emission peaks ranging from 1.7 to 8.7 kpc (e.g., Carilli et al. 2002). The more sensitive and higher spatial resolution observations that will be routinely achieved with ALMA will clarify the CO morphology of quasars.

The CO excitation conditions that have been measured in quasars have primarily been at $z \sim 2$. Barvainis et al. (1997) find that the CO is substantially excited in the Cloverleaf quasar (H1413+117, $z \sim 2.5$) through the $J = 7$ level. High–spatial resolution observations of two $z \sim 4$ quasars by Carilli et al. (2002) find similar excitation conditions in CO, both of which have multiple CO emission peaks in their morphology. More recent large velocity gradient modeling of $z \sim 4.7$ quasar BR 1202−0725 also found a CO SED that peaks at $J = 7$ (Riechers et al. 2006b). The high excitation conditions observed in quasars are indicative of extremely warm and dense molecular gas heated by ongoing star formation and are consistent with active star formation during the quasar phase.

The quasar sample of Solomon & Vanden Bout reports CO line widths in high-z quasars ranging from roughly $\sigma \sim 100$ to 250 km s^{-1} (Carilli & Wang 2006). Large-bandwidth observations with the 4 GHz COBRA correlator on OVRO by Hainline et al. (2004) of a sample of three $z = 2$–3 quasars showed similarly narrow CO line width.

While these are in apparent contrast to the large mean line widths in $z \sim 6$ quasars reported here, the narrower line widths of quasars from $2 \leq z \leq 5$ may be simply explained by the evolution of V_c with decreasing redshift. Namely, while quasars from $2 \leq z \leq 5$ appear to form in halos of comparable mass to those at $z \sim 6$ (Croom et al. 2005; Shen et al. 2007), the expected circular velocity will naturally be lower than their $z \sim 6$ analogs by a factor of $[(1 + z)/(1 + 6)]^{1/2}$. As a result, the circular velocity for these halos at $z \sim 2$ would be of order $\sigma \sim 300$–350 km s^{-1}, consistent with clustering measurements of $z \sim 2$ quasars (e.g., Croom et al. 2005; Porciani & Norberg 2006; Myers et al. 2007; Hopkins et al. 2007d) and studies of the quasar proximity effect (e.g., Faucher-Giguere et al. 2008; Kim & Croft 2007; Guimaraes et al. 2007) and slightly larger than measured CO line widths (Solomon & Vanden Bout 2005), although it is possible that there is a potential selection bias toward quasars with narrow line widths (§ 5.3) at lower redshifts as well.

In this context, we emphasize that the simulations presented here *do not* predict large ($\sigma \sim 500$–800 km s^{-1}) line widths for quasars which form at lower (e.g., $z \sim 2$) redshift, even if they form in halos of comparable mass to luminous sources at $z \sim 6$. To illustrate this, we examine the predicted CO line widths of the binary merger simulation of Narayanan et al. (2006b; also presented in Robertson et al. 2006c). The circular velocity of the progenitor galaxies was $V_c = 160$ km s^{-1}. The total mass of the progenitor galaxies in this example was $4.8 \times 10^{11}\ h^{-1}\ M_\odot$, and the final merger produced a central black hole mass of $\sim 5 \times 10^7\ h^{-1}\ M_\odot$. The σ of the unresolved CO($J = 1$–0) line profile ranges from 100 to 150 km s^{-1} during the peak of the quasar phase, over three orthogonal viewing angles, consistent

with CO line width measurements of $z \sim 2$ quasars and reflective of the host virial velocity.

These models then suggest a self-consistent picture which naturally explains the evolution of CO line widths as a function of redshift in terms of the circular velocity of the quasar host galaxy halo. Future modeling will need to quantify the extent of potential molecular disk-driven selection effects (e.g., § 5.3) for quasars at lower redshifts ($z \sim 2$–4). Indeed, other works have suggested that quasars in this redshift range may be observed at a preferred shallow range of viewing angles as evidenced by their CO line widths (e.g., Carilli & Wang 2006).

7.2. *Submillimeter Galaxies*

Submillimeter galaxies (SMGs) represent a class of massive, dusty starbursts at $z \sim 2$ largely detected by blind surveys with the SCUBA and MAMBO bolometers. Typical infrared luminosities in these sources of $\sim 10^{13}\ L_\odot$ correspond to a SFR of $\gtrsim 1000\ M_\odot$ yr^{-1}, assuming an insignificant AGN contribution (Smail 2007). X-ray and IR studies have shown that these galaxies are known to contain embedded AGNs, although their relative contribution to the bolometric luminosity is uncertain (Alexander et al. 2005a, 2005b; Donley et al. 2005; Polletta et al. 2006). Optical morphologies of SMGs indicate that many are interacting and/or mergers (Chapman et al. 2004). Recent CO morphologies and emission line profiles have furthered this scenario (Greve et al. 2005; Tacconi et al. 2006). Many studies have pointed to a picture in which SMGs may be ongoing mergers at $z \sim 2$, but in a prequasar phase (e.g., Blain et al. 2002). This combined with the fact that SMGs are the most massive and actively star-forming galaxy population at $z \sim 2$ make SMGs an interesting comparative for our simulated $z \sim 6$ quasar.

The excitation characteristics have been observed in multiple CO emission lines for only one case: $z = 2.5$ SMG SMM J16359+6612. In this galaxy, the CO flux density peaks at $J = 5$ (Weiß et al. 2005a), consistent with highly excited gas. The excitation conditions are similar to those seen in our simulations when the SFRs are comparable.

The molecular morphology in SMGs closely resembles the extended CO emission seen in simulations and observations of J1148+5251, as well as in the prequasar phase galaxy in our simulations at $z = 7$–10. The average CO FWHM radius in the recent Tacconi et al. (2006) sample is 2 kpc. The large spatial extent of CO emission in SMGs combined with an apparent lack of strong quasar activity has been interpreted as being the consequence of extremely massive and gas-rich galaxy mergers early in the evolution of the galaxy and prior to the quasar phase (e.g., Tacconi et al. 2006). Indeed, if SMGs form through hierarchical mergers, then the models presented here suggest that the spatially extended and disturbed CO morphologies seen in SMGs further indicate that these galaxies may be mergers prior to an optical quasar phase (e.g., Fig. 4).

The CO line widths of SMGs are more enigmatic. The average CO emission line from an SMG is typically about double the width of that from a quasar of similar redshifts (e.g., Carilli & Wang 2006; Greve et al. 2005; Tacconi et al. 2006). The average line width in SMGs is $\sigma \sim 330$ km s^{-1} (FWHM ~ 780 km s^{-1}), compared to a mean σ of 130 km s^{-1} seen in $z \sim 2$ quasars (Greve et al. 2005). Within the context of the models presented in this work, a number of physical motivations for these differing line widths may be at play.

First, in our models the mean line widths from galaxies with virialized cold gas are seen to roughly correspond with the circular velocity of a host halo. When comparing galaxies of similar redshifts, if SMGs are dynamically relaxed, this would imply

that SMGs may originate in more massive halos than quasars. Indeed, clustering measurements made by Blain et al. (2004) have suggested that SMGs are hosted by halos slightly larger than quasars at comparable redshifts. If SMGs reside in halos $\gtrsim 4$ times more massive than typical quasar host galaxies, the difference in CO line widths may be accounted for.

An alternative explanation for the line widths may arise from an evolutionary standpoint. Specifically, as Figure 8 shows, there is a typical drop in CO line width by a factor of ~ 2 close to the quasar phase of a merging galaxy system. This owes to gas in the violent environs of a galaxy merger becoming rotationally supported late in the evolution of the merger. If SMGs are a class of objects hosted by halos of similar mass to their quasar counterparts, then it may be that SMGs are simply massive mergers at $z \sim 2$ prior to their active quasar phase. Certainly CO line profiles and morphologies from SMGs are consistent with merging activity (Greve et al. 2005; Tacconi et al. 2006; Narayanan et al. 2006b; Narayanan et al. 2007b). Moreover, numerical simulations of merging galaxies coupled with self-consistent radiative transfer solutions have pointed to a picture in which SMGs may be mergers caught in a phase of massive black hole growth, although prior to an optical quasar phase (Chakrabarti et al. 2006).

Other authors have suggested that SMGs may be similar to quasars in their place in galaxy evolution, but simply viewed more edge-on. Carilli & Wang (2006) suggested that if these $z \sim 2$ galaxy populations are truly of the same class, then one can infer a mean viewing angle of $\sim 13°$ for quasars, whereas SMGs are more likely randomly oriented.

Finally, it may be that the CO emission properties of SMGs are not explained by physical models such as those presented in this work. If, for example, the massive star formation rates are fueled at least in part by accretion of gas from the host halo (which is seen to occur for at least some galaxies in cosmological simulations; see, e.g., Finlator et al. 2006), the CO line widths may not reflect the circular velocity of the system, at least during phases of elevated star formation, as they do in merging galaxies.

In summary, correspondence between some observed trends of molecular line emission in the models of hierarchical $z \sim 6$ quasar formation and SMGs which form at later times suggest that it is plausible that SMGs fall naturally into a merger-driven evolutionary sequence; however, at least from molecular line diagnostics alone, its location on this sequence is not completely clear. Of course, alternative scenarios cannot be ruled out here. Further models of hierarchical galaxy mergers appropriate for $z \sim 2$ will have to be examined in order to further quantify the relation of CO emission properties to the evolution of SMGs.

8. SUMMARY AND CONCLUSIONS

We have applied non-LTE radiative transfer simulations to cosmological and hydrodynamic galaxy formation simulations to predict the CO emission from representative $z \sim 6$ quasars that are modeled to form hierarchically in massive 10^{12}–$10^{13}\,M_\odot$ halos. We made predictions concerning the CO excitation patterns, morphologies, and line widths in this extreme class of objects. We further made broad comparisons to the only current CO detection at $z \gtrsim 6$, J1148+5251 at $z = 6.42$. Our main results are the following:

1. Owing to very warm and dense conditions in the molecular ISM, the CO flux density is predicted to peak at the $J = 8$ level during the early, hierarchical formation process of the quasar host galaxy ($z \sim 8$), when the SFR can be as high as $\sim 10^4\,M_\odot\,\mathrm{yr}^{-1}$.

During the peak quasar phase, the central AGN reduces the nuclear starburst, and the SFR drops to $\sim 10^2\,M_\odot\,\mathrm{yr}^{-1}$. Consequently, the CO flux density peaks at the $J = 5$–6 level. These excitation conditions are indicative of an ongoing starburst and are consistent with observations of J1148+5251. As the gas becomes more diffuse and the starburst dies down in the post-quasar phase ($z \lesssim 6$), the peak in the CO flux is predicted to drop to $J \approx 3$.

2. The CO morphologies of $z \sim 6$ quasars may exhibit multiple emission peaks during the active quasar phase, owing to separated peaks of high-density emission that have not yet coalesced. The multiple emission peaks in the morphology of the CO($J = 3$–2) gas during the quasar phase of our simulations are very similar to observations of J1148+5251 and are robust along many viewing angles. These results imply that a merger-driven formation scenario for $z \sim 6$ quasars produces CO morphologies consistent with that of J1148+5251.

3. On average, the CO line widths from quasars at $z \sim 6$ are reflective of the virial velocity of the host halo, although there exists a large sight line–dependent dispersion in line widths. During the hierarchical buildup of the host galaxy, the median line widths are roughly twice the virial velocity and settle to the virial velocity during the quasar phase. During the quasar phase, the sight line–averaged line width for the $\sim 10^{13}\,M_\odot$ halo is ~ 500–$800\,\mathrm{km\,s}^{-1}$. In the lowest mass halo ($\sim 10^{12}\,M_\odot$) the sight line–averaged line width is $\sim 300\,\mathrm{km\,s}^{-1}$.

4. A fraction of sight lines in each model is compatible with observations and is a strong function of halo mass. Specifically, the number of sight lines with narrow line widths compatible with observations increases with decreasing halo mass. The most massive $\sim 10^{13}\,M_\odot$ halo shows $\sim 2\%$–3% of sight lines compatible with observations. The $\sim 10^{12}\,M_\odot$ halo has line widths similar to observations of J1148+5251 $\sim 10\%$ of the time. The percentage of sight lines compatible with observations increase owing to selection effects (next point).

5. Quasars at $z \sim 6$ selected for optical luminosity may preferentially be in a face-on configuration, as this provides the least obscuration of the central black hole. In these configurations, the CO line widths are narrower, thus causing quasars selected for optical luminosity to preferentially have narrower line widths than their sight line–averaged values. The fraction of sight lines with line widths compatible with observations increases to 10%–25% when considering quasars selected for optical luminosity. This suggests that these models may be in agreement with observations if J1148+5251 is being observed in a face-on configuration. A direct consequence of these selection effects is that in order to observe the full dispersion in CO line widths in $z \sim 6$ quasars, observations must probe quasars with edge-on molecular disks (which are typically lower on the optical luminosity function).

6. Because of the evolution of V_c with redshift of halos of similar mass, quasars which form in $\sim 10^{12}$–$10^{13}\,M_\odot$ halos (as they are thought to; see, e.g., Croom et al. 2005; Shen et al. 2007) at lower redshift will naturally have smaller line widths, compatible with observations. We explicitly show this by examining the line widths of a binary merger simulation appropriate for present epochs. In this light, the simulations presented here *do not* predict large ($\sigma \sim 500$–$800\,\mathrm{km\,s}^{-1}$) CO line widths for quasars which form at lower redshifts, but rather a suggestive self-consistent model for the potential origin of CO line widths in quasars at both low and high redshift.

7. Our merger-driven model for quasar formation predicts a host galaxy that lies on the M_{BH}-M_{bul} relation during the active

quasar phase (Li et al. 2007; Robertson et al. 2006c; Hopkins et al. 2007c). During the hierarchical buildup of the host galaxy, the median CO line width tends to typically overestimate the dynamical mass by a factor of 2–5, as much of the gas is highly dynamical and not virialized. During the quasar phase, dynamical masses derived from the median line widths are a better representation of the true mass. There is a large range in derived dynamical masses coincident with the large sight line–dependent range of line widths seen at a given time. If selection effects are in place such that molecular disks in observed high-z quasars are typically close to face-on, CO-derived dynamical masses will preferentially underestimate the true mass unless the shallow viewing angle is accounted for.

REFERENCES

Abel, T., Bryan, G. L., & Norman, M. L. 2002, Science, 295, 93
Alexander, D. M., Bauer, F. E., Chapman, S. C., Smail, I., Blain, A. W., Brandt, W. N., & Ivison, R. J. 2005a, ApJ, 632, 736
Alexander, D. M., Smail, I., Bauer, F. E., Chapman, S. C., Blain, A. W., Brandt, W. N., & Ivison, R. J. 2005b, Nature, 434, 738
Barnes, J. E., & Hernquist, L. 1991, ApJ, 370, L65
———. 1996, ApJ, 471, 115
Barth, A. J., Martini, P., Nelson, C. H., & Ho, L. C. 2003, ApJ, 594, L95
Barvainis, R., Maloney, P., Antonucci, R., & Alloin, D. 1997, ApJ, 484, 695
Bernes, C. 1979, A&A, 73, 67
Bertoldi, F., Carilli, C. L., Cox, P., Fan, X., Strauss, M. A., Beelen, A., Omont, A., & Zylka, R. 2003a, A&A, 406, L55
Bertoldi, F., et al. 2003b, A&A, 409, L47
Blain, A. W., Chapman, S. C., Smail, I., & Ivison, R. 2004, ApJ, 611, 725
Blain, A. W., Smail, I., Ivison, R. J., Kneib, J.-P., & Frayer, D. T. 2002, Phys. Rep., 369, 111
Blitz, L., Fukui, Y., Kawamura, A., Leroy, A., Mizuno, N., & Rosolowsky, E. 2007, in Protostars and Planets V, ed. B. Reipurth, D. Jewitt, & K. Keil (Tucson: Univ. Arizona Press), 81
Bondi, H. 1952, MNRAS, 112, 195
Bondi, H., & Hoyle, F, 1944, MNRAS, 104, 273
Bromm, V., & Larson, R. B. 2004, ARA&A, 42, 79
Carilli, C. L., & Wang, R. 2006, AJ, 131, 2763
Carilli, C. L., et al. 2002, ApJ, 575, 145
———. 2005, ApJ, 618, 586
Chakrabarti, S., Cox, T. J., Hernquist, L., Hopkins, P. F., Robertson, B., Di Matteo, T. 2007, ApJ, 658, 840
Chakrabarti, S., Fenner, Y., Hernquist, L., Cox, T. J., & Hopkins, P. F. 2006, preprint (astro-ph/0610860)
Chapman, S. C., Smail, I., Windhorst, R., Muxlow, T., & Ivison, R. J. 2004, ApJ, 611, 732
Cox, T. J., Di Matteo, T., Hernquist, L., Hopkins, P. F., Robertson, B., & Springel, V. 2006a, ApJ, 643, 692
Cox, T. J., Dutta, S., Di Matteo, T., Hernquist, L., Hopkins, P. F., Robertson, B., & Springel, V. 2006b, ApJ, 650, 791
Cox, T. J., et al. 2007, ApJ, in press
Croom, S. M., et al. 2005, MNRAS, 356, 415
Davé, R., Hernquist, L., Katz, N., & Weinberg, D. H. 1999, ApJ, 511, 521
Dietrich, M., Hamann, F., Appenzeller, I., & Vestergaard, M. 2003a, ApJ, 596, 817
Dietrich, M., Hamann, F., Shields, J. C., Constantin, A., Heidt, J., Jager, K., Vestergaard, M., & Wagner, S. J. 2003b, ApJ, 589, 722
Di Matteo, T., Colberg, J., Springel, V., Hernquist, L., & Sijacki, D. 2007, ApJ, submitted (arXiv: 0705.2269)
Di Matteo, T., Springel, V., & Hernquist, L. 2005, Nature, 433, 604
Donley, J. L., Rieke, G. H., Rigby, J. R., Pérez-González, P. G. 2005, ApJ, 634, 169
Downes, D., & Solomon, P. M. 1998, ApJ, 507, 615
Fan, X., Narayanan, V. K., Strauss, M. A., White, R. L., Becker, R. H., Pentericci, L., & Rix, H. 2002, AJ, 123, 1247
Fan, X., et al. 2003, AJ, 125, 1649
———. 2004, AJ, 128, 515
Faucher-Giguere, C., Lidz, A., Zaldarriaga, M., & Hernquist, L. 2008, ApJ, in press (astro-ph/0701042)
Finlator, K., Davé, R., Papovich, C., & Hernquist, L. 2006, ApJ, 639, 672
Freudling, W., Corbin, M. R., & Korista, K. T. 2003, ApJ, 587, L67
Gao, L., White, S. D. M., Jenkins, A., Frenk, C. S., & Springel, V. 2005, MNRAS, 363, 379
Greve, T., & Sommer-Larsen, J. 2006, ApJ, submitted (astro-ph/0608683)

Greve, T. R., et al. 2005, MNRAS, 359, 1165
Guimaraes, R., et al. 2007, MNRAS, 377, 657
Haiman, Z., & Loeb, A. 2001, ApJ, 552, 459
Hainline, L. J., Scoville, N. Z., Yun, M. S., Hawkins, D. W., Frayer, D. T., & Isaak, K. G. 2004, ApJ, 609, 61
Hernquist, L. 1990, ApJ, 356, 359
Hopkins, P. F., Cox, T. J., Keres, D., & Hernquist, L. 2007a, ApJ, submitted (astro-ph/0706.1246)
Hopkins, P. F., & Hernquist, L. 2006, ApJS, 166, 1
Hopkins, P. F., Hernquist, L., Cox, T. J., Di Matteo, T., Martini, P., Robertson, B., & Springel, V. 2005a, ApJ, 630, 705
Hopkins, P. F., Hernquist, L., Cox, T. J., Di Matteo, T., Robertson, B., & Springel, V. 2005b, ApJ, 630, 716
———. 2005c, ApJ, 632, 81
———. 2006a, ApJS, 163, 1
Hopkins, P. F., Hernquist, L., Cox, T. J., & Keres, D. 2007b, ApJ, submitted (astro-ph/0706.1243)
Hopkins, P. F., Hernquist, L., Cox, T. J., Robertson, B., Di Matteo, T., & Springel, V. 2006b, ApJ, 639, 700
Hopkins, P. F., Hernquist, L., Cox, T. J., Robertson, B., & Krause, E. 2007c, ApJ, 669, 67
Hopkins, P. F., Hernquist, L., Cox, T. J., Robertson, B., & Springel, V. 2006c, ApJS, 163, 50
Hopkins, P. F., Hernquist, L., Martini, P., Cox, T. J., Robertson, B., Di Matteo, T., & Springel, V. 2005d, ApJ, 625, L71
Hopkins, P. F., Lidz, A., Hernquist, L., Coil, A. L., Myers, A. D., Cox, T. J., & Spergel, D. N. 2007d, ApJ, 662, 110
Hopkins, P. F., Richards, G. T., & Hernquist, L. 2007e, ApJ, 654, 731
Hopkins, P. F., Somerville, R., Hernquist, L., Cox, T. J., Robertson, B., & Li, Y. 2006d, ApJ, 652, 864
Hoyle, F., & Lyttleton, R. A. 1939, Proc. Cambridge Philos. Soc., 34, 405
Jiang, L., et al. 2006, AJ, 132, 2127
Katz, N., Weinberg, D. H., & Hernquist, L. 1996, ApJS, 105, 19
Kennicutt, R. 1998, ApJ, 498, 541
Keres, D., Yun, M. S., & Young, J. S. 2003, ApJ, 582, 659
Kim, Y.-R., & Croft, R. 2007, MNRAS, in press (astro-ph/0701012)
Lee H-H., Bettens, R. P. A., & Herbst, E. 1996, A&AS, 119, 111
Li, Y., et al. 2007, ApJ, 665, 187
Lidz, A., Hopkins, P. F., Cox, T. J., Hernquist, L., & Robertson, B. 2006, ApJ, 641, 41
Magorrian, J., et al. 1998, AJ, 115, 2285
Maiolino, R., et al. 2005, A&A, 440, L51
Marconi, A., & Hunt, L. K. 2003, ApJ, 589, L21
McKee, C. F., & Ostriker, J. P. 1977, ApJ, 218, 148
Mihos, J. C., & Hernquist, L. 1994, ApJ, 425, L13
———. 1996, ApJ, 464, 641
Myers, A. D., Brunner, R. J., Nichol, R. C., Richards, G. T., Schneider, D. P., & Bahcall, N. A. 2007, ApJ, 658, 85
Narayanan, D., Cox, T. J., Shirley, Y., Dave, R., Hernquist, L., & Walker, C. K. 2007a, preprint (astro-ph/0711.1361)
Narayanan, D., Kulesa, C., Boss, A. P., & Walker, C. K. 2006a, ApJ, 647, 1426
Narayanan, D., et al. 2006b, ApJ, 642, L107
———. 2007b, preprint (astro-ph/0710.0384)
Pelupessy, F. I., Di Matteo, T., & Ciardi, B. 2007, ApJ, 665, 107
Press, W. H., & Schechter, P. 1974, ApJ, 187, 425
Polletta, M., et al. 2006, ApJ, 642, 673
Porciani, C., & Norberg, P. 2006, MNRAS, 371, 1824

Riechers, D. A., Walter, F., Carilli, C., Weiß, A., Bertoldi, F., Menten, K., Knudsen, K., & Cox, P. 2006a, ApJ, 645, L13

Riechers, D. A., et al. 2006b, ApJ, 650, 604

Robertson, B., Bullock, J., Cox, T. J., Di Matteo, T., Hernquist, L., Springel, V., & Yoshida, N. 2006a, ApJ, 645, 986

Robertson, B., Cox, T. J., Hernquist, L., Franx, M., Hopkins, P. F., Martini, P., Springel, V, 2006b, ApJ, 641, 21

Robertson, B., Hernquist, L., Cox, T. J., Di Matteo, T., Hopkins, P. F., Martini, P., & Springel, V. 2006c, ApJ, 641, 90

Robertson, B., Li, Y., Cox, T. J., Hernquist, L., & Hopkins, P. F. 2007, ApJ, 667, 60

Rosolowsky, E. 2005, PASP, 117, 1403

———. 2006, ApJ, 674, 240

Schmidt, M. 1959, ApJ, 129, 243

Schöier, F. L., van der Tak, F. F. S., van Dishoeck, E. F., & Black, J. H. 2005, A&A, 432, 369

Seljak, U., & Zaldarriaga, M. 1996, ApJ, 469, 437

Shen, Y., et al. 2007, AJ, 133, 2222

Sheth, R. K., & Tormen, G. 2002, MNRAS, 329, 61

Shields, G.,A., Menezes, K. L., Massart, C. A., Vanden Bout, P. 2006, ApJ, 641, 683

Sijacki, D, Springel, V., Di Matteo, T., & Hernquist, L. 2007, MNRAS, 380, 877

Smail, I. 2007, in Infrared Diagnostics of Galaxy Evolution, ed. R.-R. Chary, in press (astro-ph/0603635)

Solomon, P. M., Rivolo, A. R., Barrett, J., & Yahil, A. 1987, ApJ, 319, 730

Solomon, P. M., & Vanden Bout, P. 2005, ARA&A, 43, 677

Springel, V. 2005, MNRAS, 364, 1105

Springel, V., Di Matteo, T., & Hernquist, L. 2005a, MNRAS, 361, 776

———. 2005b, ApJ, 620, L79

Springel, V., & Hernquist, L. 2002, MNRAS, 333, 649

———. 2003a, MNRAS, 339, 289

———. 2003b, MNRAS, 339, 312

———. 2005, ApJ, 622, L9

Springel, V., et al. 2005, Nature, 435, 629

Tacconi, L. J., et al. 2006, ApJ, 640, 228

van Zadelhoff, G-J., et al. 2002, A&A, 395, 373

Volonteri, M., & Rees, M. J. 2005, ApJ, 633, 624

Walker, C. K., Adams, F. C., & Lada, C. J. 1990, ApJ, 349, 515

Walter, F., Carilli, C., Bertoldi, F., Menten, K., Cox, P., Lo, K. Y., Fan, X., & Strauss, M. 2004, ApJ, 615, L17

Walter, F., et al. 2003, Nature, 424, 406

Wang, R., et al. 2007, AJ, 134, 617

Weiß, A., Downes, D., Walter, F., & Henkel, C. 2005a, A&A, 440, L45

Weiß, A., Walter, F., & Scoville, N. Z. 2005b, A&A, 438, 533

Willott, C. J., McLure, R. J., & Jarvis, M. J. 2003, ApJ, 587, L15

Wu, J., Evans, N. J., II, Gao, Y., Solomon, P. M., Shirley, Y. L., & Vanden Bout, P. A. 2005, ApJ, 635, L173

Wu, X-B. 2007, ApJ, 657, 177

Yoshida, N., Omukai, K., Hernquist, L., & Abel, T. 2006, ApJ, 652, 6